General Models for the Electrochemical Hydrogen Oxidation and Hydrogen Evolution Reactions – Theoretical Derivation and Experimental Results Under Near Mass-Transport Free Conditions

Anthony R. Kucernak[*], and Christopher Zalitis[†]

Department of Chemistry, Imperial College London, United Kingdom

Abstract

Full derivations of Heyrovsky-Volmer (HV), Tafel-Volmer(TV), Heyrovsky-Tafel(HT), and Heyrovsky-Tafel-Volmer(HTV) mechanisms under steady state conditions are provided utilising a new theoretical framework which allows better understanding of the each of the mechanistic currents and part currents. Simple and easily implemented equations are presented, which provide both the hydrogen coverage and electrochemical current as a function of overpotential and relevant kinetic parameters. It is shown how these responses are governed by a set of dimensionless parameters associated with the ratio of electrokinetic parameters. For each of the different mechanisms, an "atlas" of H_{ads} coverage with overpotential and corresponding current density is provided, allowing an understanding of all possible responses depending on the dimensionless parameters. Analysis of these mechanisms provides the limiting reaction orders of the exchange current density for protons and bimolecular hydrogen for each of the different mechanisms, as well as the possible Tafel slopes as a function of the molecular symmetry factor, β. Only the HV mechanism is influenced by pH whereas the TV,HT, and HTV mechanisms are not. The cases where the equations simplify to limiting forms are discussed. Analysis of the exchange current density from experimental data is discussed, and it is shown that fitting the linear region around the equilibrium potential underestimates the true exchange current density for all of the mechanisms studied. Furthermore, estimates of exchange current density via back-extrapolation from large overpotentials is also shown to be highly inaccurate. Analysis of Tafel slopes is discussed along with the mechanistic information which can and cannot be determined. The new models are used to simultaneously fit sixteen experimental responses of Pt/C electrodes in acid towards the *her/hor* as a function of η, pH, $p(H_2)$, and temperature, using a consistent set of electrokinetic parameters. Examples of implementation of the equations as both computable document format and Excel spreadsheets are provided.

[*] Corresponding author: Phone: +44 20 75945831, E-mail: anthony@imperial.ac.uk

[†] Current Address: Johnson Matthey Technology Centre, Blounts Court Road, Sonning Common, Reading, RG4 9NH, UK.

1 Introduction

The hydrogen oxidation reaction (*hor*) and hydrogen evolution reaction (*her*) are of great technological importance due to the increasing need to store renewable energy in a suitable chemical form(i.e. via electrolysis to hydrogen) and conversion back to electrical energy (i.e. via fuel cells). Over the last several years there has been increasing interest in these reactions because of the development of a range of different materials capable of being used within electrolysers to replace platinum[1-4]. At the same time there has been significant desire to understand the *hor* on platinum as the performance measured within fuel cells is typically much greater than that measured using standard electrochemical techniques such as the rotating disk electrode (RDE)[5]. There has been some progress to understanding the mass transport effects by developing new approaches which allow faster transport of hydrogen to the catalyst[6-9]. However, there is also a marked decrease in performance of the *hor* under alkaline conditions[10], which would appear to be counter to the standard mechanisms, most of which suggest that the reaction should be pH independent. The development of new theoretical computational frameworks for understanding the thermodynamics of these reactions is producing intriguing suggestions[11]. Most of the attempts at understanding the electrochemical kinetics of the *her/hor* can be traced to the pioneering work of Tafel, Heyrovsky and Volmer [12-14], within which a number of elementary steps were demarcated, Table 1.

Table 1 Description of the different equations used in solution of the hydrogen oxidation/evolution reaction and the time dependence of hydrogen coverage for each individual equation. S = surface adsorption site. $H_{2,surf}$ is a hydrogen molecule adjacent to the surface.

$H_{2,surf} + 2S \rightarrow 2S\text{-}H_{ad}$	k_{ad}	Eq 1	Tafel
$2S\text{-}H_{ad} \rightarrow H_{2,surf} + 2S$	k_{des}	Eq 2	
$H_{2,surf} + S \rightarrow S\text{-}H_{ad} + H^+ + e^-$	k_1	Eq 3	Heyrovsky
$S\text{-}H_{ad} + H^+ + e^- \rightarrow H_{2,surf} + S$	k_{-1}	Eq 4	
$S\text{-}H_{ad} \rightarrow S + H^+ + e^-$	k_2	Eq 5	Volmer
$S + H^+ + e^- \rightarrow S\text{-}H_{ad}$	k_{-2}	Eq 6	

Although various approaches have been used to try and extract useful electrokinetic data from the experimental *her/hor* results, for the most part these have involved mathematical treatments of Eq 1-Eq 6 in which simplifications have been introduced to make the resulting formulations tractable.

For instance Vogel *et al* analysed hydrogen oxidation on porous Pt electrodes assuming a Tafel-Volmer mechanism[15]. For the hydrogen oxidation reaction, they derived a current-potential relationship under the assumption of simple charge transfer kinetics (i.e. a Butler-Volmer type approximation), assuming a Tafel-Volmer reaction with slow hydrogen adsorption. The latter aspect was based on their experimental measurements of low-pressure gas phase H_2/D_2 exchange over platinum (i.e. in the absence of electrolyte) which yielded a first order rate constant at 295 K of 2.4 cm s^{-1}. In their derivation, they assumed that $\theta_{H_{ad}}/\theta_{H_{ad}}^{\mathrm{eq}}$ (the relative variation of the hydrogen coverage away from the equilibrium potential) did not change significantly within 50mV of the equilibrium potential (this assumption will be discussed below)

$$i = i_0 \left[1 - \frac{c_{\mathrm{H2}}}{c^0_{\mathrm{H2}}} \mathrm{e}^{2f\eta} \right] \qquad \text{Eq 7}$$

$$f = \frac{\mathrm{F}}{RT}$$

In fact, this equation captures an essential feature of the *hor/her* that many attempts to fit experimental data using the Butler-Volmer expression (or simple modifications of it) fail to capture – and that is that the current does not show an exponential increase at positive overpotentials (*hor*), but instead tends to "flatten out". In contrast, at negative overpotentials (*her*) there is an exponential increase in current. In many papers, this "flattening out" has been interpreted as due to a mass transport limitation, however the effect remains even in systems with very high rates of mass transport, suggesting that it is an intrinsic aspect of the electrokinetics[16-19].

In more recent work, initially by Chialvo et al[20-25] and also taken up by others[26-27] have attempted to produce suitable kinetic equations to describe the electrokinetics of Eq 1-Eq 6. These have then been used to rationalise experimental data. Such attempts to model the *hor*/*her* have not attempted to determine an explicit analytical expression for hydrogen coverage as a function of the reaction kinetics, but have typically relied on approximations, or assumptions on the equilibrium coverage of hydrogen. For instance, in [28], the coverage of hydrogen is calculated by numerical methods requiring an assumption as to the coverage of hydrogen under equilibrium conditions. In [27] an approximate solution to the hydrogen coverage is determined under certain conditions, but an assumption must still be made about the equilibrium coverage of hydrogen. In [19] the hydrogen coverage as a function of potential is calculated from the H_{upd} charge assuming a Frumkin isotherm. In the former cases it is usually assumed that the equilibrium coverage of hydrogen is very low, and simulations have suggested values over a very wide range: 0.07-10^{-7}, although there is significant variation in the literature and in some cases, e.g. especially the *her*, this coverage may be quite high. Indeed, a recent study gives an equilibrium hydrogen coverage of 0.179[29], which is somewhat different to values of ca. 10^{-3} used in previous studies by the same authors[28]. The inability to determine suitable values of hydrogen coverage under equilibrium conditions, and indeed over the entire potential range from the *her* region to the *hor* region limits the applicability of models to one particular aspect – e.g. *hor* or *her*. In such models the equilibrium coverage is a parameter used to improve the fit to data without providing any descriptive information. Clearly, a model which can deal with both *her* and *hor* is not only more powerful, but also more likely to represent an accurate portrayal of reality, and some progress has been made in that area[30].

Within this paper we consider a new conceptual electrokinetic framework for treating the *her* and *hor* in a material independent way over a range of different conditions and apply this framework to the reaction on platinum in order to determine the material-dependent kinetic parameters for the *hor/her* on that material. The benefit of our approach compared to previous approaches is that the parameters used in the rate equations link directly to the elementary steps, and thus allow insight into both the surface coverage of intermediates and intrinsic rates of the different reactions occurring on the surface. We consider the analytical solutions to the Tafel Volmer (TV), the Heyrovsky-Volmer (HV), the Heyrovsky-Tafel (HT), and the Heyrovsky-Tafel-Volmer (HTV) reactions. The full Tafel-Heyrovsky-Volmer model is shown to reduce to the TV and HT mechanisms under suitable limiting assumptions. For each of the different models we survey the entire spectrum of H_{ads} isotherms and j-η plots. In doing so we provide a

useful “atlas” of possible electrokinetic responses. These may be useful in assessing the hydrogen reaction over a range of different electrocatalytic systems. For each of the different mechanisms we provide information about the possible Tafel slopes of the linear sections of the $log|j|vs\ \eta$-plots. We show how the exchange current densities of the reactions are related to the underlying kinetic equations, and how use of data from the micropolarisation region underestimates the true exchange current density (in contrast to the Butler-Volmer equation). We then show how these kinetic equations can be used to fit mass-transport free electrokinetic data for Pt/C in acid electrolytes. In order to aid interpretation and understanding of these different mechanisms we provide dynamic “computable document format” examples of each of the mechanisms.

2 Experimental

A commercial 60 wt.% Pt/C catalyst (HiSPEC 9100, Alfa Aesar, metal area of 89 $m^2\ g^{-1}$ [31]) and high purity gases (N_2, H_2 and O_2 at >5.8 N from Air Products) with 6 N rated regulators (GCE DruVa) and acids were used; perchloric acid from VWR (Merc Suprapur) and GFS chemicals (Veritas double distilled) were both used with negligible difference in performance (not shown). Ultra pure water (Millipore Milli-Q, 18.2 MΩ cm) was used in producing all electrolytes. Before the electrochemical measurements, all glassware were soaked in acidified potassium permanganate over 8 h, rinsed with acidified hydrogen peroxide and then rinsed at least six times with ultra pure water. All floating electrodes were cleaned in a soxhlet extractor with ultra pure water for 24 hours before use.

Electrochemical measurements were performed with a Gamry Reference 600 potentiostat in a water jacketed three electrode electrochemical cell utilizing a Pt counter electrode and a RHE in a Luggin capillary configuration. The cell was held at the relevant temperature using a re-circulator (Polyscience digital temperature controller, ±0.1 ^oC).

For RDE measurements, an aqueous 0.1 M $HClO_4$ solution was used as the electrolyte. Pt rotating disk electrodes with a diameter of 5 mm (AFE2M050PT, PINE instruments) which are applicable up to 7000 rpm were used as the WE. The RDE was attached to a modulated speed rotator (AFMSRCE, PINE instruments).

The floating electrodes were made up and conditioned as described in [17, 32]. The electrodes were floated on liquid electrolytes with the reactant gas supplied to the catalyst through the hydrophobised pores, allowing high mass transport. 0.5 or 4 mol dm^{-3} perchloric acid was used – the latter to minimise the uncompensated resistance at the high currents achieve from the HOR. Gas mixtures were obtained using gas flow controllers (Bronkhurst EL flow series). Uncompensated resistances were corrected using the high frequency intercept of impedance measurements at a range of voltages.

3 Theoretical approach

An example of the results we obtain for each of the different cases we have studied is provided in Figure 1 where we give ***indicative*** steady state voltammograms (these are not meant to be examples of *hor/her* on any specific metal, but rather are given to illustrate the characteristic form of the resultant equations), plotting the hydrogen coverage

at the same time. We also provide, in an inset in each graph, a Tafel plot[†] i.e . a plot of $|\log j|$ versus η. Also displayed in these $log|j|vs\ \eta$-plots are a breakdown as to the different current components – i.e. the magnitude of the appropriate reactions Eq 3-Eq 6 as a function of overpotential. We will examine the family of possible responses for each of the different mechanisms in greater detail below, but there are a number of interesting observations. For the Heyrovsky-Volmer reaction, Figure 1 (a), a number of different slopes in the $log|j|vs\ \eta$-plots are possible, depending on how the hydrogen coverage is changing over that particular potential range. No limiting current is seen in the plot. For the Tafel-Volmer reaction, Figure 1(b), a current limitation is seen during the *her* and *hor* and no clear linear region is seen in the $log|j|vs\ \eta$ plot. For Figure 1(c), the HT mechanism, a current limitation may be seen either during the *her* or during the *hor* (but not both) depending on the precise parameters used. For the HT mechanism, the hydrogen coverage always increases with increasing potential. Limiting slopes in the $log|j|vs\ \eta$-plots may be seen in either side of the reaction. In contrast, the HTV reaction, Figure 1(d), may show plateaus during either the *hor* or *her* (or both), but at large overpotentials, the current always reverts to a "Tafel" –like response.

In some approaches to model the *hor/her* reaction, the "net reaction" for each coupled step (k_1/k_{-1}, and k_2/k_{-2} etc) is calculated by taking the difference between the rates of the forward and reverse reactions, and all reactions are scaled to the magnitude of this net reaction at equilibrium (at equilibrium, there is no net reaction but two equal and opposite half reactions) e.g. see ref [24, 28, 30]. For systems which only have one major reaction step, or for which one reaction step is much slower than all others, this is a useful method as it allows the definition of an exchange current density for the reaction. For more complicated reactions, this may not be possible. Furthermore, although the approach of writing total rates has some benefits, it also suffers in that the coupling between the forward and reverse reactions is implicit in the derivation, and the parameters which are derived are the net rates of reaction, rather than the explicit rate constants themselves. Our approach is slightly different in that we want to analyse and understand explicit relationships for equilibrium hydrogen coverage, and the different rate constants, and so we evaluate the individual constants. This leads to a minimum number of parameters which retain their mechanistic relevance whilst retaining a self-consistent thermodynamic interpretation. It also allows us to examine the exchange current density in terms of the fundamental kinetic parameters.

The approach we take to solve the four different cases is rather straightforward. In the first instance we write down the kinetic expressions associated with changes to the hydrogen coverage for each of the different mechanisms ($\frac{d\theta_{H_{ad}}}{dt}$, Table 2) which is then set to zero as appropriate for the steady state approximation, and the equation is solved for $\theta_{H_{ad}}$. In this approach the adsorption isotherm of hydrogen is presumed to be Langmuirian – that is there are no interactions on the surface, we do not (necessarily) assume participation of upd hydrogen, and furthermore this model is not capable of determining the coverage of upd hydrogen (see [19] for a discussion of the difference between the H_{ad} kinetic intermediate, H_{upd}, and H_{opd}). Rather, our approach is to assess a kinetic set of expressions for the *hor/her* and assess how well they replicate experimental data. From this assessment we will be able to determine whether further modifications to the kinetic expressions are necessary. In doing so we produce a set of

[†] Hence forth we will use the term "$log|j|vs\ \eta$-plot" instead of "Tafel plot" to avoid confusion with the Tafel mechanism.

equations with the minimum number of free parameters so as to make sure that our system is not overparameterised. Following determination of the hydrogen coverage with potential, we determine the coverage of hydrogen under equilibrium conditions. The $\theta_{H_{ad}}(\eta)$ term is then inserted into the electrochemical kinetic equation (j/F, Table 2) to produce the electrochemical rate equation. At the equilibrium potential, the net current is zero, and so the electrochemical equation may be solved in order to eliminate one of the variables. Substitution into the electrochemical equation provides the final solution. We assume transport of hydrogen and protons to the electrode surface is fast – i.e. we ignore mass transport effects. We will later on compare these models to our recent experimental results utilising low loading electrodes under high mass-transport[16-17, 33]. Computational document format (cdf) documents of each of the mechanisms derived are available to down load as part of the supplementary information. The data used for generating the experimental plots, and spreadsheets which allow fitting of data to each of the mechanisms is available for download[34].

3.1 Heyrovsky-Volmer Reaction

Solution of the steady-state adsorbed hydrogen coverage (Table 1) yields a simple expression for $\theta_{H_{ad}}^{HV}$(where the superscript represents the associate reaction)

$$\theta_{H_{ad}}^{HV} = \frac{a_{\mathrm{H2}}k_1 + a_{H^+}k_{-2}}{a_{\mathrm{H2}}k_1 + k_2 + a_{H^+}k_{-1} + a_{H^+}k_{-2}} \qquad \text{Eq 8}$$

Where a_{H_2}, a_{H^+} are respectively the proton and hydrogen activities at the electrode surface with the standard state chosen to be the same as used to define the equilibrium potential.

The analytical expression for θ_{Had} is then substituted into the kinetic expression for the electrochemical current based on the steps associated with an electrochemical reaction (Table 1). Under equilibrium conditions, there is no net reaction. Furthermore, because of the requirement that $\frac{d\theta_{H_{ad}}^{HV}}{dt}$ =0, both the Heyrovsky and Volmer reactions (i.e. k_1/k_{-1} and k_2/k_{-2}) must independently also show no net reaction (indeed, they must have the same reversible potential), and so we have

$$\theta_{H_{ad}}^{\mathrm{HV,eq}} = \frac{a_{\mathrm{H2}}k_1^{\mathrm{eq}} + a_{H^+}k_{-2}^{\mathrm{eq}}}{a_{\mathrm{H2}}k_1^{\mathrm{eq}} + k_2^{\mathrm{eq}} + a_{H^+}k_{-1}^{\mathrm{eq}} + a_{H^+}k_{-2}^{\mathrm{eq}}} \qquad \text{Eq 9}$$

$$\left(k_1^{\mathrm{eq}}a_{H_2}\left(1-\theta_{H_{ad}}^{\mathrm{HV,eq}}\right) - k_{-1}^{\mathrm{eq}}a_{H^+}\theta_{H_{ad}}^{\mathrm{HV,eq}} + k_2^{\mathrm{eq}}\theta_{H_{ad}}^{\mathrm{HV,eq}} - k_{-2}^{\mathrm{eq}}a_{H^+}\left(1-\theta_{H_{ad}}^{\mathrm{HV,eq}}\right)\right) = 0 \qquad \text{Eq 10}$$

Where k_i^{eq} is the value of the rate constant, k_i, for reaction *i* under equilibrium conditions, i.e. when η=0, and under a defined value of a_{H^+} and a_{H_2}.

For the Heyrovsky-Volmer reaction, it is not possible to independently solve Eq 9 and Eq 10 for k_{-1} in terms of k_1 and k_{-2} in terms of k_2 as there is a coupling between both sets of equations through $\theta_{H_{ad}}^{\mathrm{HV,eq}}$. The solution of Eq 9 and Eq 10 give the following constraint on the solution:

$$\frac{k_2^{eq}}{k_{-2}^{eq}a_{H^+}} = \frac{k_{-1}^{eq}}{k_1^{eq}}\frac{a_{H^+}}{a_{\mathrm{H2}}}$$ Eq 11

Hence we define, a constant K, such that

$$K = \frac{k_2^{eq}}{k_{-2}^{eq}a_{H^+}} \quad \therefore \quad k_{-2}^{eq} = \frac{k_2^{eq}}{Ka_{H^+}}, \qquad k_{-1}^{eq} = Kk_1^{eq}\frac{a_{\mathrm{H2}}}{a_{H^+}}$$ Eq 12

Substitution of k_{-1}^{eq}, and k_{-2}^{eq} into Eq 9 provides the equilibrium coverage of hydrogen in terms of our explicit parameters

$$\theta_{H_{ad}}^{HV,eq} = \frac{1}{1+K}$$ Eq 13

and we find that the hydrogen coverage under equilibrium conditions is pH dependent (implicit in the definition of K, Eq 12), but independent of bimolecular hydrogen activity. In previous approaches, $\theta_{H_{ad}}^{HV,eq}$ was an explicit fitting parameter, whereas in our case it is a derived parameter from the electrokinetic rate constants.

Incorporation of deviations away from equilibrium though a perturbing electrochemical overpotential are then introduced in the normal manner. The rate constants under equilibrium conditions are related to the equilibrium potential and the intrinsic rate constant for each of the forward and reverse reactions as described in Appendix A.

The symmetry factors for the reactions are associated exclusively with single one-electron transfer steps participating in a multistep electrode process[35]. We assume the β values for anodic and cathodic reactions sum to one, and for simplicity assume the same symmetry factor for both the Heyrovsky and Volmer steps. We assume that the anodic and cathodic transfer coefficients sum to one. Hence in Eq 8 we make the following substitutions

$$k_1 = k_1^{eq}e^{\beta f\eta},$$
$$k_{-1} = Kk_1^{eq}\frac{a_{\mathrm{H2}}}{a_{H^+}}e^{-(1-\beta)f\eta},$$
$$k_2 = k_2^{eq}e^{\beta f\eta},$$
$$k_{-2} = \frac{k_2^{eq}}{Ka_{H^+}}e^{-(1-\beta)f\eta} \qquad f = \frac{\mathrm{F}}{RT}$$ Eq 14

where $\eta = E - E^{eq}$. Substitution and simplification for the overpotential dependence of $\theta_{H_{ad}}^{\mathrm{HV}}(\eta)$ provides

$$\theta_{H_{ad}}^{\mathrm{HV}}(\eta) = \frac{(Ge^{f\eta}+1)}{(Ge^{f\eta}+1)+\mathrm{K}(e^{f\eta}+G)}$$ Eq 15

Where $G = \frac{Kk_1^{\mathrm{eq}}a_{\mathrm{H2}}}{k_2^{\mathrm{eq}}}$ is a derived parameter associated with the ratio of the two forward reactions and the magnitude of the forward and reverse Volmer reaction. Because a common value of β is used for both sets of equations, all terms containing β cancel out. As will be seen below, this isotherm has a particularly rich set of responses and may find advantageous uses in describing other electrochemical systems in which adsorption of intermediates occurs. $\theta_{H_{ad}}^{\mathrm{HV}}(\eta)$ shows some interesting properties, and is affected by both pH and bimolecular hydrogen activity. A typical response for $\theta_{H_{ad}}^{\mathrm{HV}}(\eta)$ is shown in Figure 1 (a), along with the calculated current density.

This figure allows comparison of representative responses for the different mechanisms examined in this paper in terms of their hydrogen coverage and current density. The limiting solutions for Eq 15 as $\eta \to \infty$, and $\eta \to -\infty$ are

$$\lim_{\eta \to -\infty} \theta_{H_{ad}}^{\mathrm{HV}}(\eta) = \frac{1}{1+GK} \qquad \lim_{\eta \to \infty} \theta_{H_{ad}}^{\mathrm{HV}}(\eta) = \frac{1}{1+\frac{K}{G}} \qquad \text{Eq 16}$$

We find that the hydrogen coverage at large positive and negative overpotentials does not necessarily approach one and zero, respectively, but instead depend on the balance of the electrochemical constants. The variation of the hydrogen isotherm with different values of the dimensionless constants, G and K, are displayed in Figure 2. When G=1 the hydrogen coverage is potential independent, and $\theta_{H_{ad}}^{\mathrm{HV}}(\eta) = \frac{1}{1+K}$, Figure 2(a). This corresponds to the situation where the forward rates are equal ($k_1^{\mathrm{eq}} a_{\mathrm{H2}} = k_2^{\mathrm{eq}}$) and, as the hydrogen coverage is at steady state, this also means that both reverse rates are also equal ($k_{-1}^{eq} = k_{-2}^{eq}$). The actual value of the hydrogen coverage is then determined by K which provides a measure of whether the forward or reverse Volmer reactions are more favoured (this then also applies to the Heyrovsky reaction as both reactions are coupled). When K=1, Figure 2(a), the hydrogen coverage shows symmetry about the equilibrium potential with $\theta_{H_{ad}}^{\mathrm{HV}}(\eta) = (1 - \theta_{H_{ad}}^{\mathrm{HV}}(-\eta))$. The shape of the isotherms are controlled by G, and values of G greater than one produce a hydrogen coverage which increases with potential, which is counter to the normal expectation. Such a situation occurs when the forward and reverse Heyrovsky reactions are fast, but the forward and reverse Volmer reaction are slow. Under these conditions, adsorbed hydrogen builds up on the surface as the forward Volmer reaction is unable to keep up with the forward Heyrovsky reaction. Because the forward/reverse Heyrovsky reactions are fast, the surface is kept clear of adsorbed hydrogen at low potentials. With values of G less than one, adsorbed hydrogen coverage increase with decreasing potential. This situation occurs when the Volmer reactions are fast, but the Heyrovsky reactions are slow, and hence there is a buildup of hydrogen on the surface as potential is decreased. Two other plots of hydrogen coverage as a function of the model parameters are shown in Figure 2. In Figure 2(b) constant value of G is used and K is varied. As G<1, hydrogen coverage increases as potential is decreased (what would be considered the normal situation), and the value of K controls either the lower bounds of hydrogen coverage (K>1, $\eta \to \infty$), or the upper bounds of hydrogen coverage (K<1, $\eta \to -\infty$), in line with the limits described in Eq 16. When a constant ratio of G to K is used, it is possible to vary the position of the isotherm, shifting to more positive or negative values, as displayed in Figure 2 c. When G=100, and G=10^6K (i.e. the inverse of the values used in Figure 2 b&c), the plots in Figure 2 b&c remain the same, but they are reflected in the η=0 line (not shown).

Expansion of the electrochemical kinetic equations provides the following equation for current density as a function of $K, k_1^{eq} k_2^{eq}, \beta$:

$$j^{HV}(\eta) = F\left(\left(k_1^{eq} a_{H_2}\left(1 - \theta_{H_{ad}}^{\mathrm{HV}}(\eta)\right) + k_2^{eq}\theta_{H_{ad}}^{\mathrm{HV}}(\eta)\right)e^{\beta f \eta} - \left(Kk_1^{eq} a_{\mathrm{H2}}\theta_{H_{ad}}^{\mathrm{HV}}(\eta) + \frac{k_2^{eq}}{K}\left(1 - \theta_{H_{ad}}^{\mathrm{HV}}(\eta)\right)\right)e^{-(1-\beta)f\eta}\right) \qquad \text{Eq 17}$$

This simplifies to the more compact expression in terms of *K* and *G*

$$j^{HV}(\eta) = F\left(\frac{2Gk_2^{eq}e^{-(1-\beta)f\eta}\left(e^{2f\eta}-1\right)}{(Ge^{f\eta}+1)+K(e^{f\eta}+G)}\right) \qquad \text{Eq 18}$$

Compared to the definition of $\theta_{H_{ad}}^{\mathrm{HV}}(\eta)$ in Eq 15, Eq 18 contains k_2^{eq} in its derivation, but scaled current densities may be produced for the same values of K, and G used in Eq 15

$$\frac{j^{HV}(\eta)}{k_2^{eq}} = F\left(\frac{2G\left(e^{(1+\beta)f\eta}-e^{-(1-\beta)f\eta}\right)}{(Ge^{f\eta}+1)+K(e^{f\eta}+G)}\right) \qquad \text{Eq 19}$$

Plots of the scaled currents for the hydrogen coverages in Figure 2(a),(b) and (c) are provided in Figure 2(d),(e) and (f). When *K*=1, performance on the anodic and cathodic branches are the same with the best response obtained for larger values of *G*. This corresponds to the presumed situation operating in efficient *hor/her* catalysts – at negative overpotentials, the surface is covered with adsorbed hydrogen and at positive overpotentials, the surface is free of adsorbed hydrogen. When the reverse is true (i.e. G<1), the performance decreases. There is an ultimate limit approached when K=1 and G>>1 or G<<1 at which point the current approaches a "classical" limit, with a response that looks similar to the Butler-Volmer equation

$$j^{HV}(\eta) \cong F\left(2k_1^{\mathrm{eq}}a_{\mathrm{H2}}\left(e^{\beta f\eta}-e^{-(1-\beta)f\eta}\right)\right) \qquad \text{K} \cong 1,\ \text{G}<<1 \qquad \text{Eq 20}$$

Or when G >>1

$$j^{HV}(\eta) \cong F\left(2k_2^{\mathrm{eq}}\left(e^{\beta f\eta}-e^{-(1-\beta)f\eta}\right)\right) \qquad \text{K} \cong 1,\ \text{G}>>1 \qquad \text{Eq 21}$$

That is the current is limited by **either** the Heyrovsky **or** the Volmer reactions during both the *hor* and *her.* The slopes of the $log|j|vs\ \eta$-plots show characteristic values of βF/RT and –(1-β)F/RT V decade^{-1}. However, even in these cases Eq 20 and Eq 21 are rather poor representations of Eq 19 close to the equilibrium potential, overestimating the expected current. This comes about as close to the equilibrium potential, the denominator of Eq 19 becomes dominated by $(KG+1)$. Many papers interpret hydrogen oxidation in terms of equations similar to Eq 20[36], although it is important to note this equation only holds when K=1 (rates of forward/reverse Heyrovsky are the same), and the rate of the forward Volmer is at least ten times greater than the rate of the forward Heyrovsky (G/K << 1). Also, this equation does not hold so well close to the equilibrium potential. In our fitting results for the micropolarisation region of the Heyrovsky-Volmer mechanism on Platinum in our previous paper[32], we found that the forward Volmer is about the same order of magnitude as the forward Heyrovsky, and that K is somewhat greater than 1, suggesting that the use of Eq 20 or Eq 21 to fit data using platinum as a catalyst may not be optimum. Furthermore, as will be discussed below, when a full HV fit to the data over an expanded potential region is performed, the required fitting parameters diverge even more from the requirements for simplification to Eq 20 or Eq 21.

When K≠1, the responses can be quite different as shown in Figure 2 (e) and (f) which correspond to the hydrogen coverages in Figure 2(b) and(c). Variation of K away from one leads to asymmetry in the *her/hor* reactions. The

slopes of the $log|j|vs\ \eta$-plots may not only show the characteristic values of β and –(1-β) (both multiplied by F/RT), but may also show values of (1+β) and –(2-β). Enhanced slopes occur

(a) at anodic potentials when both *G* and *K* <<1, and hence the denominator in Eq 18 and Eq 19 tends to one. In this case both the forward Heyrovsky and forward Volmer reactions are slow compared to their reverse reactions;

(b) at cathodic potentials when either *G* or *K* (or both) >>1 so that the denominator in Eq 18 and Eq 19 tend to $Ge^{f\eta}, Ke^{f\eta}$ or the sum of those two terms. In this case the forward Volmer or forward Heyrovsky reactions are fast relative to their reverse reactions.

It is important to note that the regions in which higher slopes are seen might suggest that the *hor*/*her* are enhanced in these regions, but in reality, performance in these regions is less than what might be expected by back-extrapolating the performance from larger overpotentials. Hence, these regions underperform compared to what might be expected. In the example in Figure 1 (a), the *her* branch looks to be much more active than the *hor* branch, and if one assumed a "Butler-Volmer" potential dependence then this might presume that this shift is due to a value of α somewhat less than the usually expected value of 0.5. In reality, this increased slope of the $log|j|vs\ \eta$-plot is due to K>>1. As was mentioned previously, many models assume that the hydrogen coverage ($\theta_{H_{ad}}^{\mathrm{HV}}/\theta_{H_{ad}}^{\mathrm{HV,eq}}$) does not change significantly around the equilibrium potential (e.g. [15]). For the HV model this only happens when G≈1 (hydrogen coverage is potential independent as Heyrovsky and Volmer steps proceed at the same rate) or when K<G and KG < 1 (i.e. hydrogen coverage is large around the equilibrium potential as the forward Volmer and reverse Heyrovsky steps are slow compared to the other reactions).

In order to further illustrate the kinetic equations a computable document format (cdf) representation of the Heyrovsky-Volmer equations as a function of overpotential and the parameters G, K, k_2^{eq} and β is provided in the supporting information (note that a_{H2} and a_{H^+} are implicitly included in *G,* and *K*). This allows interactive plots of current density, $log|j|vs\ \eta$ plots (including the ½ currents for each component), and $\theta_{H_{ad}}^{\mathrm{HV}}(\eta)$. The phenomenological anodic and cathodic α values[†] as a function of potential are calculated by explicitly differentiating the logarithm of the absolute value of Eq 17. Plots of this function (multiplied by F/RT) provide horizontal plateaus representing the values of α_a, and α_c in the anodic and cathodic regions, and also provide useful information as to the regions over which such a slope would be visible (i.e. the horizontal plateau):

$$\alpha_a, \alpha_c = \frac{RT}{F}\frac{\partial log_e|j|}{\partial \eta} \qquad \text{Eq 22}$$

As we know the value of β used to generate the plots, we can then understand how the mechanisms transforms the single electron transfer β into the value which we measure (α).

[†] The phenomenologically measured α values are linked to the symmetry factors, β, for the one electron transfer through the specific mechanism35. Guidelli, R.; Compton, R. G.; Feliu, J. M.; Gileadi, E.; Lipkowski, J.; Schmickler, W.; Trasatti, S., Defining the Transfer Coefficient in Electrochemistry: An Assessment (Iupac Technical Report). *Pure and Applied Chemistry* **2014**, *86*, 245-258..

3.2 Tafel-Volmer Reaction

Solution of the Tafel-Volmer equation is performed in a similar manner to the Heyrovsky-Volmer using the appropriate equations for $\frac{d\theta_{H_{ad}}^{\mathrm{TV}}}{dt}$ and *j* in Table 2. Solution of the steady-state adsorbed hydrogen coverage yields a quadratic expression for $\theta_{H_{ad}}^{\mathrm{TV}}$, and with two possible equations for $\theta_{H_{ad}}^{\mathrm{TV}}$

$$\theta_{H_{ad}}^{\mathrm{TV}} = \frac{4a_{\mathrm{H2}}k_{\mathrm{ad}} + k_2 + k_{-2}a_{H^+} \pm \sqrt{{k_2}^2 + 2k_2(4a_{\mathrm{H2}}k_{\mathrm{ad}} + k_{-2}a_{H^+}) + 16k_{\mathrm{ad}}k_{\mathrm{des}}a_{\mathrm{H2}} + k_{-2}a_{H^+}(k_{-2}a_{H^+} + 8k_{\mathrm{des}})}}{4a_{\mathrm{H2}}k_{\mathrm{ad}} - 4k_{\mathrm{des}}} \quad \text{Eq 23}$$

Only one of the roots (the negative branch) gives a physically relevant response and this is then combined with the equation for current generation (Table 2). Under equilibrium conditions, the net rate is zero, and $\theta_{H_{ad}}^{\mathrm{TV}}$ is replaced by its equilibrium form with all constants in their equilibrium form

$$j^{\mathrm{TV}} = F\left(k_2^{eq}\theta_{H_{ad}}^{\mathrm{TV},eq} - k_{-2}^{eq}a_{H^+}\left(1 - \theta_{H_{ad}}^{\mathrm{TV},eq}\right)\right) = 0 \quad \text{Eq 24}$$

Substitution of $\theta_{H_{ad}}^{\mathrm{TV},eq}$ into Eq 24 and solving for k_{-2}^{eq} provides a quadratic in k_{-2}^{eq} with two solutions:

$$k_{-2}^{eq} = \pm\frac{\mathrm{B}k_2^{eq}}{a_{H^+}} \quad \text{Eq 25}$$

where the parameter $B = \sqrt{\frac{a_{\mathrm{H2}}k_{\mathrm{ad}}}{k_{\mathrm{des}}}}$ is associated with the ratio of the forward and reverse Tafel reaction.

Only the positive root makes physical sense. As the expansion of k_{-2}^{eq} has a_{H^+} in the denominator and all instances of k_{-2} are multiplied by a_{H^+}, it is found that unlike the HV equation, the shape of $\theta_{H_{ad}}^{\mathrm{TV},eq}(\eta)$ is pH independent. Expansion of the k_2 and k_{-2} terms as previously discussed for the HV reaction produces

$$k_2 = k_2^{eq}e^{\beta f\eta},$$
$$k_{-2} = \frac{\mathrm{B}k_2^{eq}}{a_{H^+}}e^{-(1-\beta)\eta f} \quad \text{Eq 26}$$

Substitution into Eq 23 results in the potential dependent coverage of hydrogen on the electrode surface

$$\theta_{H_{ad}}^{\mathrm{TV}}(\eta) = \frac{4B^2 + \mathrm{Z}\left(e^{\beta f\eta} + Be^{-(1-\beta)f\eta}\right) - \sqrt{16\mathrm{B}^2 + \left(Z\left(e^{\beta f\eta} + Be^{-(1-\beta)f\eta}\right)\right)^2 + 8BZ\left(Be^{\beta f\eta} + e^{-(1-\beta)f\eta}\right)}}{4(B^2 - 1)} \quad \text{Eq 27}$$

Where $Z = \frac{k_2^{\mathrm{eq}}}{k_{\mathrm{des}}}$ which balances H_{ads} recombination compared to its electrochemical reaction. The hydrogen coverage is pH independent, but affected by the chemical adsorption/desorption rate constants and the bimolecular hydrogen concentration. $\theta_{H_{ad}}^{\mathrm{TV}}(\eta)$ is controlled by the two dimensionless constants, *B* and Z. The denominator of Eq 27 disappears as $a_{\mathrm{H2}}k_{\mathrm{ad}} \to k_{\mathrm{des}}$, although taking $\lim_{a_{\mathrm{H2}}k_{\mathrm{ad}} \to k_{\mathrm{des}}} \theta_{H_{ad}}^{\mathrm{TV}}(0) = \frac{1}{2}$ leads to the conclusion that at that point the hydrogen coverage is ½ at all potentials. $\theta_{H_{ad}}^{\mathrm{TV}}(\eta)$ is bounded between 0 and 1, and always decreases with increasing η. A plateau in the value of $\theta_{H_{ad}}^{\mathrm{TV}}$ may occur at $\eta = 0$ when $Z << B^2$ i.e. when the Volmer forward reaction is slower

than the Tafel reaction. Under these conditions, the assumption that $\theta_{H_{ad}}^{\mathrm{HV}}/\theta_{H_{ad}}^{\mathrm{HV,eq}}$ does not change significantly close to the equilibrium potential is reasonable. Under equilibrium conditions (η=0) we obtain

$$\theta_{H_{ad}}^{\mathrm{TV},eq} = \frac{1}{1+\frac{1}{\mathrm{B}}} \qquad \text{Eq 28}$$

And hence the equilibrium coverage is only dependent on the adsorption/desorption rate constants and not the Volmer reaction. Modification of the electrochemical rate equation to take into account the substitution for k_2 and k_{-2} and substitution of $\theta_{H_{ad}}^{\mathrm{TV}}(\eta)$ gives

$$j^{\mathrm{TV}}(\eta) = Fk_2^{eq}\left(\theta_{H_{ad}}^{\mathrm{TV}}(\eta)e^{\beta f\eta} - \mathrm{B}\left(1-\theta_{H_{ad}}^{\mathrm{TV}}(\eta)\right)e^{-(1-\beta)f\eta}\right) \qquad \text{Eq 29}$$

The resulting equation provides electrochemical current density in terms of the parameters k_{ad}, k_{des}, k_2^{eq} and β. The TV equation for the hydrogen reaction is thus pH independent, unlike the HV equation. As with the HV reaction, it is possible to plot j^{TV} in terms of the dimensionless constants *B,* and *Z*, by taking Eq 29 and dividing by k_{des}

$$\frac{j^{\mathrm{TV}}(\eta)}{k_{\mathrm{des}}} = FZ\left(\theta_{H_{ad}}^{\mathrm{TV}}(\eta)e^{\beta f\eta} - B\left(1-\theta_{H_{ad}}^{\mathrm{TV}}(\eta)\right)e^{-(1-\beta)f\eta}\right) \qquad \text{Eq 30}$$

An example of a solution to this equation is provided in Figure 1(b) utilising values of parameters representative of those required to fit experimental observations. The Tafel-Volmer reaction shows a limiting current at suitably high overpotentials, both during the *hor* and *her*. This limiting current is associated with limitations of both the adsorption ($j^{TV}(\eta\to\infty) = 2Fk_{des}B^2 = 2Fa_{\mathrm{H2}}k_{\mathrm{ad}}$) and desorption ($j^{TV}(\eta\to-\infty) = 2Fk_{\mathrm{des}}$) processes during the Tafel reaction, Eq 1 and Eq 2. For the example shown, no clear slope is seen in the $log|j|vs\ \eta$ plot (inset), although the individual Volmer components of the current show linear regions in the $log|j|vs\ \eta$ plots at large overpotentials. It is interesting that both Volmer ½ currents show a peaked response with a maximum current at the position at which $\theta_{H_{ad}}^{\mathrm{TV}}(\eta) = \frac{1}{2}$. Plots mapping out a larger part of the (*Z*,*B*) parameter space are provided in Figure 3. As with the HV case, a large number of different isotherms for the hydrogen adsorption coverage are seen. When Z<<B (Forward Tafel reaction is faster than forward Volmer reaction) a plateau in hydrogen coverage is seen at the equilibrium potential, Figure 3a. Only once the overpotential is sufficiently far away from the equilibrium potential does $\theta_{H_{ad}}^{\mathrm{TV}}(\eta)$ tend to one and zero at negative and positive overpotentials, respectively. When B<<Z (Tafel step slower than Volmer step) then a more characteristic isotherm is seen, Figure 3c. In the intermediate regime, a mixture of these two behaviours is possible, Figure 3b. Casual inspection of Eq 29 would suggest that there is something amiss with the expression as no hydrogen concentration term is associated with the *hor* branch of the reaction, but it is associated with the *her* part of the curve through *B*. Part of this confusion is resolved by considering that $\theta_{H_{ad}}^{\mathrm{TV}}(\eta)$ contains a_{H2} in its derivation. A second aspect of Eq 29 is that it is not immediately obvious is that it forces an adsorption and desorption rate limitation to the *hor* and *her* respectively. This arises from the finite values of k_{ad} and k_{des}, and occurs through the fine balance of the preexponential coverage term and the exponential driving force term. As can be seen from the scaled current densities corresponding to the hydrogen coverages, Figure 3d-f, a range of different current responses are possible. When one or both of the Volmer steps

are sufficiently slow compared to the Tafel steps, then it is possible to obtain plots with a linear region evident in the $log|j| vs\ \eta$ plot, Figure 3d-e. These typically have slopes which can be used to extract α_{eff}. When the Volmer reaction is fast, and the forward and reverse Tafel reactions have the same magnitude, then no linear region is evident, and there is a continuous curvature to the $log|j| vs\ \eta$ plots until limitations due to the Tafel step leads to a plateau in current. In the case where there is a significant mismatch in rates between the forward and reverse Tafel reactions, then it is possible to have a linear region in the $log|j| vs\ \eta$ plots. These correspond to the overpotentials where the hydrogen coverage is rapidly changing, and show slopes of ±2 (multiplied by F/RT), Figure 3f. In order to further illustrate the kinetic equations a computable document format (cdf) representation of the Tafel-Volmer equations as a function of overpotential is provided in the supporting information. This allows interactive plots of current density, $log|j| vs\ \eta$ plots (including the ½ currents for each component), $\theta_{H_{ad}}^{\text{TV}}$, and $\frac{RT}{F}\frac{\partial|\log j|}{\partial\eta} vs\ \eta$ plots (effective symmetry factor plots) as a function of the parameters *B,Z,* and β.

3.3 Heyrovsky-Tafel Reactions

An interesting case arises if one considers just the Heyrovsky and Tafel reactions, and assumes the Volmer reaction cannot occur. Under this condition, adsorbed hydrogen produced during the oxidation of molecular hydrogen must be removed by recombination in the reverse Tafel reaction. During the *hor* the net reaction is

$$H_{2,surf} + S \rightarrow S\text{-}H_{ad} + H^+ + e^- \qquad \text{Eq 31}$$

$$2S\text{-}H_{ad} \rightarrow H_{2,surf} + 2S \qquad \text{Eq 32}$$

During the *her* there is then the requirement for initial adsorption of hydrogen before subsequent reaction with a proton

$$H_{2,surf} + 2S \rightarrow 2S\text{-}H_{ad} \qquad \text{Eq 33}$$

$$S\text{-}H_{ad} + H^+ + e^- \rightarrow H_{2,surf} + S \qquad \text{Eq 34}$$

Counterintuitively, hydrogen evolution is required during the *hor* in order to keep the hydrogen coverage constant, and hydrogen adsorption is required during the *her* for the same reason. Although this process might be considered as somewhat "theoretical", it has been invoked for hydrogen evolution in alkaline media [37]. Solving for the steady state hydrogen coverage, and substituting into the current production relationship (Table 2), and solving for k_{-1}^{eq} provides the following

$$k_{-1}^{eq} = \pm\frac{\sqrt{a_{\text{H2}}}\sqrt{k_{\text{des}}}k_1^{\text{eq}}}{a_{\text{H}^+}\sqrt{k_{\text{ad}}}} = \frac{k_{\text{des}}Y}{a_{\text{H}^+}B} \qquad \text{Eq 35}$$

where $Y = \frac{a_{\text{H2}}k_1^{\text{eq}}}{k_{\text{des}}}$ represents the balance between the forward Heyrovsky and reverse Tafel reactions. Substitution into the steady state equation for hydrogen coverage and simplification provides the steady-state hydrogen coverage as a function of potential for the Heyrovsky-Tafel reaction, $\theta_{H_{ad}}^{\text{HT}}(\eta)$

$$\theta_{H_{ad}}^{\text{HT}}(\eta) = \frac{4B^2 + \text{Y}\left(e^{\beta f\eta} + \frac{e^{-(1-\beta)f\eta}}{B}\right) - \sqrt{16\text{B}^2 + \left(\text{Y}\left(e^{\beta f\eta} + \frac{e^{-(1-\beta)f\eta}}{B}\right)\right)^2 + 8Y\left(e^{\beta f\eta} + Be^{-(1-\beta)f\eta}\right)}}{4(B^2-1)} \qquad \text{Eq 36}$$

Under equilibrium conditions, the coverage of hydrogen is controlled by B in the same manner as for the Tafel-Volmer reaction and hence is dependent only on k_{ad}, k_{des} and the bimolecular hydrogen concentration and is independent of proton concentration

$$\theta_{H_{ad}}^{\mathrm{HT},eq} = \frac{1}{1+\frac{1}{\mathrm{B}}} \qquad \text{Eq 37}$$

$\theta_{H_{ad}}^{\mathrm{HT}}$ is bounded by 0, and 1, and always **increases** with potential (Figure 4), although it may show a plateau at η=0 for $Y << B^2$, i.e when the Heyrovsky forward reaction rate is much slower than the Tafel step (see example in Figure 1c). Substitutions of k_{-1}^{eq} into the equation for the electrochemical current and subsequent simplification gives

$$j^{\mathrm{HT}}(\eta) = Fk_1^{eq}\left(a_{H_2}\left(1-\theta_{H_{ad}}^{\mathrm{HT}}(\eta)\right)e^{\beta f\eta} - \frac{\sqrt{a_{\mathrm{H2}}}\sqrt{k_{\mathrm{des}}}}{\sqrt{k_{\mathrm{ad}}}}\theta_{H_{ad}}^{\mathrm{HT}}(\eta)e^{-(1-\beta)f\eta}\right) \qquad \text{Eq 38}$$

a dimensionless current in terms of the parameters *B* and *Y* may then be obtained i.e. the same parameters as used to define the hydrogen coverage in Eq 36

$$\frac{j^{\mathrm{HT}}(\eta)}{k_{\mathrm{des}}} = FY\left(\left(1-\theta_{H_{ad}}^{\mathrm{HT}}(\eta)\right)e^{\beta f\eta} - \frac{\theta_{H_{ad}}^{\mathrm{HT}}(\eta)}{\mathrm{B}}e^{-(1-\beta)f\eta}\right) \qquad \text{Eq 39}$$

Limiting currents are always seen at sufficiently large anodic and cathodic overpotentials, although at intermediate potentials it is possible to have regions in which the slopes of the $\frac{\mathrm{RT}}{F}\frac{d\mathrm{Log}_e|j|}{\mathrm{d}\eta}$ vs η plots have α_{eff} values which correspond to β or 2 for the anodic section and –(1- β) or -2 for the cathodic section. These cases are highlighted in Figure 4.

3.4 Heyrovsky-Tafel-Volmer Reactions

Solution of the Heyrovsky-Tafel-Volmer equation is performed in a similar manner to the previous cases above using the appropriate equations for $\frac{d\theta_{H_{ad}}^{\mathrm{HTV}}}{dt}$ and *j* in Table 2. Solution of the steady-state adsorbed hydrogen coverage yields a quadratic expression for $\theta_{H_{ad}}^{\mathrm{HTV}}$, and with two possible solutions for $\theta_{H_{ad}}^{\mathrm{HTV}}$, with only the negative branch making physical sense

$$\begin{aligned}&\theta_{H_{ad}}^{\mathrm{HTV}}\\ &= \frac{1}{4(a_{\mathrm{H2}}k_{\mathrm{ad}}-k_{\mathrm{des}})}\left(k_2+a_{\mathrm{H2}}(k_1+4k_{\mathrm{ad}})+a_{H^+}(k_{-1}+k_{-2})\right.\\ &\left.\pm\sqrt{\left(k_2+a_{\mathrm{H2}}(k_1+4k_{\mathrm{ad}})+a_{H^+}(k_{-1}+k_{-2})\right)^2-8(a_{\mathrm{H2}}(k_1+2k_{\mathrm{ad}})+a_{H^+}k_{-2})(a_{\mathrm{H2}}k_{\mathrm{ad}}-k_{\mathrm{des}})}\right)\end{aligned} \qquad \text{Eq 40}$$

Under equilibrium conditions the net current is zero

$$j^{\mathrm{HTV}} = F\left(k_1^{\mathrm{eq}}a_{H_2}\left(1-\theta_{H_{ad}}^{\mathrm{HTV,eq}}\right)-k_{-1}^{\mathrm{eq}}a_{H^+}\theta_{H_{ad}}^{\mathrm{HTV,eq}}+k_2^{\mathrm{eq}}\theta_{H_{ad}}^{\mathrm{HTV,eq}}-k_{-2}^{\mathrm{eq}}a_{H^+}\left(1-\theta_{H_{ad}}^{\mathrm{HTV,eq}}\right)\right)=0 \qquad \text{Eq 41}$$

and hence it is possible to solve for k_{-1}^{eq} in terms of k_1^{eq} and k_{-2}^{eq} in terms of k_2^{eq}

$$k_{-1}^{\mathrm{eq}} = \frac{\sqrt{a_{\mathrm{H2}}}\sqrt{k_{\mathrm{des}}}k_1^{\mathrm{eq}}}{a_{H^+}\sqrt{k_{\mathrm{ad}}}} = \frac{Yk_{\mathrm{des}}}{Ba_{H^+}},$$
$$k_{-2}^{\mathrm{eq}} = \frac{\sqrt{a_{\mathrm{H2}}}\sqrt{k_{\mathrm{ad}}}k_2^{\mathrm{eq}}}{\sqrt{k_{\mathrm{des}}}a_{H^+}} = \frac{Bk_2^{\mathrm{eq}}}{a_{H^+}} \qquad \text{Eq 42}$$

Substitution into Eq 40 leads to the potential dependence of $\theta_{H_{ad}}^{\mathrm{HTV}}(\eta)$ in terms of $k_1^{\mathrm{eq}}, k_2^{\mathrm{eq}}, k_{\mathrm{ad}}, k_{\mathrm{des}}, \beta$. We find that the coverage is controlled by the three dimensionless constants previously defined, *B, Y* and *Z*, and that the equation for coverage can be rewritten in terms of these parameters

$$\theta_{H_{ad}}^{\mathrm{HTV}}(\eta) = \frac{1}{4(\mathrm{B}^2-1)}\left(4\mathrm{B}^2 + \mathrm{Z}\left(e^{\beta\eta} + \mathrm{B}e^{(-1+\beta)\eta}\right) + \mathrm{Y}\left(e^{\beta\eta} + \frac{1}{\mathrm{B}}e^{(-1+\beta)\eta}\right) - \sqrt{\left(4\mathrm{B}^2 + \mathrm{Z}(e^{\alpha\eta} + \mathrm{B}e^{(-1+\beta)\eta}) + \mathrm{Y}\left(e^{\beta\eta} + \frac{1}{\mathrm{B}}e^{(-1+\beta)\eta}\right)\right)^2 - 8(\mathrm{B}^2-1)(2\mathrm{B}^2 + \mathrm{Y}e^{\beta\eta} + \mathrm{BZ}e^{(-1+\beta)\eta})}\right) \qquad \text{Eq 43}$$

The hydrogen coverage shows features similar to those of the HV and TV/HT mechanisms. Setting $k_1^{\mathrm{eq}} \to 0$ (i.e. no Heyrovsky reaction, $\mathrm{Y} \to 0$) produces $\theta_{H_{ad}}^{\mathrm{TV}}(\eta)$ (Eq 27). Setting $k_2^{\mathrm{eq}} \to 0$ (i.e. no Volmer reaction, $\mathrm{Z} \to 0$) produces $\theta_{H_{ad}}^{\mathrm{HT}}(\eta)$ (Eq 36). At the equilibrium potential, the hydrogen coverage simplifies to

$$\theta_{H_{ad}}^{\mathrm{HTV},eq} = \frac{1}{1+\frac{1}{\mathrm{B}}} \qquad \text{Eq 44}$$

that is, the same form of equilibrium coverage as for the Tafel-Volmer and Heyrovsky-Tafel equations. In contrast to the HV equation (but similar to the TV equation), the HTV equation is pH independent. Furthermore, when $Y = BZ$, the hydrogen coverage becomes potential independent, that is $\theta_{H_{ad}}^{\mathrm{HTV}}(\eta) = \frac{1}{1+\frac{1}{\mathrm{B}}}$ (cf the HV mechanism). When $Y > BZ$ then the hydrogen coverage increases as the potential becomes more negative (TV like behaviour) whereas when $Y < BZ$ the hydrogen coverage increases with increasing positive overpotential (such a behaviour was also seen under certain conditions for both the HV, and HT cases). This occurs when the recombination steps are fast, but the oxidation of the adsorbed hydrogen is slow. $\theta_{H_{ad}}^{\mathrm{HTV}}(\eta)$ can show limiting values at high overpotentials, similar to the case of the HV reaction. The limiting solutions for Eq 43 as $\eta \to \infty$, and $\eta \to -\infty$ are

$$\lim_{\eta\to-\infty}\theta_{H_{ad}}^{\mathrm{HTV}}(\eta) = \frac{1}{1+\frac{Y}{Z\,B^2}} \qquad \lim_{\eta\to\infty}\theta_{H_{ad}}^{\mathrm{HTV}}(\eta) = \frac{1}{1+\frac{Z}{Y}} \qquad \text{Eq 45}$$

$\theta_{H_{ad}}^{\mathrm{HTV}}(\eta)$ can also show a plateau around η=0 (as seen for the TV and HT equations).

Some representative plots of $\theta_{H_{ad}}^{\mathrm{HTV}}(\eta)$ as a function of the parameters *B, Y* and *Z* are displayed in Figure 5(a)-(c). The parameters were chosen in such a way as to exemplify the range of possible isotherms. For all isotherms shown, it is possible to produce their associated mirror images (i.e. their reflection in the y-axis).

Substitution of $\theta_{H_{ad}}^{\mathrm{HTV}}(\eta)$ into the equation for electrochemical current and simplification in line with the different parameters produces

$$j^{\mathrm{HTV}}(\eta) = F\left(\left(k_1^{\mathrm{eq}} a_{H_2}\left(1-\theta_{H_{ad}}^{\mathrm{HTV}}(\eta)\right)+k_2^{\mathrm{eq}}\theta_{H_{ad}}^{\mathrm{HTV}}(\eta)\right)e^{\beta f\eta}-\left(\frac{\sqrt{a_{\mathrm{H2}}}\sqrt{k_{\mathrm{des}}}k_1^{\mathrm{eq}}}{\sqrt{k_{\mathrm{ad}}}}\theta_{H_{ad}}^{\mathrm{HTV}}(\eta)+ Bk_2^{\mathrm{eq}}\left(1-\theta_{H_{ad}}^{\mathrm{HTV}}(\eta)\right)\right)e^{(-1+\beta)f\eta}\right) \quad \text{Eq 46}$$

As with the previous cases, it is possible to obtain a dimensionless current by dividing the current density by k_{des} as was the case with the TV and HT models. This then gives us the dimensionless current density in terms of the three parameters used to describe the hydrogen coverage: *B, Y* and *Z.*

$$\frac{j^{\mathrm{HTV}}(\eta)}{k_{\mathrm{des}}} = F\left(\left(Y\left(1-\theta_{H_{ad}}^{\mathrm{HTV}}(\eta)\right)+Z\theta_{H_{ad}}^{\mathrm{HTV}}(\eta)\right)e^{\beta f\eta}-\left(\frac{Y}{B}\theta_{H_{ad}}^{\mathrm{HTV}}(\eta)+B\,Z\left(1-\theta_{H_{ad}}^{\mathrm{HTV}}(\eta)\right)\right)e^{(-1+\beta)f\eta}\right) \quad \text{Eq 47}$$

Compared to the HV and TV situations described above, we have a more complicated parameter space to map out. Setting $k_1^{\mathrm{eq}} \to 0$ in Eq 47 (or more specifically $\mathrm{Y} \to 0$) recovers the TV equation (Eq 29) and setting $k_2^{\mathrm{eq}} \to 0$ in Eq 47 (or more specifically $Z \to 0$) recovers the HT equation, Eq 40. The HTV equation for electrochemical current is pH independent, like the TV and HT equations, but unlike the HV equation.

Scaled currents $\left(\frac{j^{\mathrm{HTV}}}{k_{\mathrm{des}}}\right)$ for the parameter sets used to plot the $\theta_{H_{ad}}^{\mathrm{HTV}}$ values in Figure 5(a)-(c) are shown in Figure 5(d)-(f). As might be expected, the scaled currents show a range of different responses similar to those seen in the HV, TV, and TH cases. A specific feature of the HTV mechanisms is that the current response can show an inflection, something not seen in any of the other mechanisms. The inflection has been used to aid fitting of experimental data which show a similar feature, and indeed this inflection has been used as proof of transition from Tafel-Volmer to Heyrovsky-Volmer kinetics[25, 27, 38]. However, it now appears that the inflection seen in the experimental data is a manifestation of two reaction sites as seen in data produced using our new experimental technique[16-17, 32] and suggested by us previously[19]. At large overpotentials the HTV mechanism always becomes dominated by the HV mechanisms as the electrokinetic steps out run the Tafel chemical step. However, closer to the equilibrium potential it is possible to have a current which is enhanced above those expected from an extrapolation from large overpotentials due to the significant involvement of the Tafel step.

In order to illustrate this last point, it is interesting to consider the proportion of current which proceeds through each of the different mechanistic steps as a function of the parameters *B,Y,* and *Z.* The current through each of the different steps as a function of overpotential may be calculated by

$$\mathrm{j_{Heyrovsky}}(\eta) = Fk_{\mathrm{des}}\left(Y\left(1-\theta_{H_{ad}}^{\mathrm{HTV}}(\eta)\right)e^{\beta f\eta}-\frac{Y}{B}\theta_{H_{ad}}^{\mathrm{HTV}}(\eta)e^{(-1+\beta)f\eta}\right) \quad \text{Eq 48}$$

and

$$\mathrm{j_{Volmer}}(\eta) = Fk_{\mathrm{des}}\left(Z\theta_{H_{ad}}^{\mathrm{HTV}}(\eta)e^{\beta f\eta}-B\,Z\left(1-\theta_{H_{ad}}^{\mathrm{HTV}}(\eta)\right)e^{(-1+\beta)f\eta}\right) \quad \text{Eq 49}$$

For the Heyrovsky and Volmer steps respectively. For the Tafel reaction we can calculate the "virtual current" associated with hydrogen reaction on the surface from mass balance arguments as

$$\mathrm{j}_{\mathrm{Tafel}}(\eta) = 2Fk_{\mathrm{des}}\left(B^2\left(1-\theta_{H_{ad}}^{\mathrm{HTV}}(\eta)\right)^2 - \left(\theta_{H_{ad}}^{\mathrm{HTV}}(\eta)\right)^2\right) \quad \text{Eq 50}$$

Eq 48-Eq 50 represent the current generated through each of the different steps, however they do not represent the proportion of current generated through each *pathway* (combination of steps). This is arguably a more important parameter as it allows us to understand the ratio of the different pathways for the *her/hor*, and how those pathways change with overpotential. We can calculate this function by recognising that $\left(1-\frac{j_{Tafel}(\eta)}{j^{\mathrm{HTV}}(\eta)}\right)$ represents the amount of reaction which proceeds through the HV pathway (i.e. the total fraction of current which does not involve the Tafel step). Hence we can deconvolute the fraction of reaction which proceeds through the different pathways as:

$$\mathrm{X}_{\mathrm{Heyrovsky-Volmer}}(\eta) = 1-\frac{j_{Tafel}(\eta)}{j^{\mathrm{HTV}}(\eta)} \quad \text{Eq 51}$$

The remaining current must pass through either the HT or TV pathways. The proportion of reaction that proceeds through those pathways is then

$$\mathrm{X}_{\mathrm{Heyrovsky-Tafel}}(\eta) = \frac{j_{Heyrovsky}(\eta)}{j^{HTV}(\eta)} - {}^1\!/_2\,\mathrm{X}_{\mathrm{Heyrovsky-Volmer}}(\eta) \quad \text{Eq 52}$$

and

$$\mathrm{X}_{\mathrm{Tafel-Volmer}}(\eta) = \frac{j_{Volmer}(\eta)}{j^{HTV}(\eta)} - {}^1\!/_2\,\mathrm{X}_{\mathrm{Heyrovsky-Volmer}}(\eta) \quad \text{Eq 53}$$

In Figure 5(g)-(i) we show examples of this breakdown for one of the sets of parameters used in Figure 5(a)-(h). It is interesting to see that the fraction of the TV pathway always peaks close to the equilibrium potential (although not necessarily exactly at the equilibrium potential) and then decays away as the overpotential increases on either side. The *HT* pathway, always shows a negligible fraction of current for all parameters considered.

3.5 Exchange current density

The exchange current density is a parameter often used to characterise complex multistep electrochemical reactions by analogy with the parameter determined from the Butler-Volmer equation. At its heart, this parameter measures how facile the electrochemical reaction is at the equilibrium potential. For the Butler-Volmer formalism, this parameter provides extra information as the large overpotential performance of the reaction (in the absence of mass transport effects) can be determined from the exchange current density and the Tafel slope. For the Butler-Volmer equation, the exchange current can be determined either by back extrapolation of the Tafel region to the equilibrium potential (either from the anodic or cathodic branches), fitting of the curve over the intermediate potential regime, or from the micropolarisation region by taking the first terms of the series expansion of the Butler-Volmer equation and fitting the slope. This latter approach is useful as it can be applied at low overpotentials, where it is often assumed that mass transport losses are not too great. All four approaches mathematically provide the same value of the exchange current density for an electrokinetic reaction following the Butler-Volmer equation.

It is often tacitly assumed that the same approach can be applied to multistep reactions, and that each of the different methods described above will provide the same numerical value of the exchange current density. As will be shown below, this is not the case and the assumption that the exchange current density can be determined from e.g. fitting the micropolarisation region, is not valid. Indeed, the utility of the exchange current density is somewhat devalued for multistep reactions, as it can no longer be assumed that the exchange current density and a Tafel slope can be used to predict currents far from the equilibrium potential (or conversely, that a Tafel slope can be used to predict the current close to the equilibrium potential). For each of the hydrogen mechanisms, we have calculated the mathematical form of the "exchange current" using each of the different approaches described above for each of the different mechanisms. The results are summarised in Table 3. In this table, we also list the mathematical equation for the equilibrium hydrogen coverage, whether the mechanism shows a pH dependence (that is if the exchange current density has a dependence on pH), and the observable Tafel slopes in terms of β.

3.5.1 "True" Exchange current density

In Table 3 we list the "true" exchange current density for each of the reactions by taking the appropriate equations (Eq 17 for HV, Eq 29 for TV, Eq 38 for HT and Eq 46 for HTV) and determining the anodic and cathodic currents when η=0, and $\theta_{H_{ad}}(\eta) = \theta_{H_{ad}}^{\mathrm{eq}}$ for the respective reaction.

For the HV mechanism, the exchange current density is associated with the serial combination of the Heyrovsky and Volmer steps. The reaction order for protons may vary between -1 to 1 dependent on the magnitude of k_1^{eq} and k_2^{eq}. Indeed, Bagotzky and Osetrova found a value of 0.5 using platinum microelectrodes although their interpretation for this non-integral value was associated with the presence of two pathways associated with the initial discharge step, one being pH dependent[6]. In our previous paper we found a reactant order for protons on Pt/C catalyst of 0.4 in the pH range 1 to -0.8. This value was adequately explained with a specific set of values for k_1^{eq} and k_2^{eq} which would result in a reaction order for protons of 0 at pH<-1, and a reaction order of 1 at pH>1 with the intermediate regime showing a continuous change of reaction order with pH[32]. The significant decrease in exchange current density for the *hor* on platinum and other metals in alkaline environments may be associated with this variation of exchange current with pH[39-40], although it may also be associated with a change of mechanism at high pH. Although a reaction order for protons less than zero is possible, the conditions under which this may occur are rather unlikely. The reaction order for bimolecular hydrogen varies between 0 and 1 depending on the magnitude of the forward Heyrovsky reaction compared to the reverse Volmer reaction. In our previous paper on the hor/her on platinum, we showed how the phenomenologically measured reaction order of hydrogen of 0.68 (quite close to the value of 0.61 measured in an alkaline environment[41]) could be rationalised in terms of the HV reaction mechanism and fitted values of k_1^{eq} and k_2^{eq} which were rather similar to each other and which thus provided results which were in the intermediate regime[32]. It is often assumed that a simplified form of the Butler Volmer equation can be used (c.f. Eq 20, Eq 21), but this requires severe constraints on the kinetic parameters which are unlikely to be satisfied.

For the TV mechanism, the exchange current is dependent on the electrochemical Volmer rate constant, k_2^{eq}, and (through its dependence on the equilibrium hydrogen coverage, $\theta_{H_{ad}}^{TV,eq}$) the parameter *B,* associated with hydrogen

adsorption on the catalyst surface. There is no pH dependence of the exchange current density and the reaction order for hydrogen varies between 0 and ½. The low value of the reaction order comes about because hydrogen adsorption is a chemical step (and hence not included in the exchange current), and the exchange current is influenced by $\theta_{H_{ad}}^{\mathrm{eq}}$ which in turn is affected by the chemical adsorption step. This is different to the case of the micropolarisation region and indeed the entire electrokinetic response which will be affected by the hydrogen activity by a different reaction order as the chemical step is then also included (see below). Thus, although the limiting current will show a first order dependence with hydrogen partial pressure, the exchange current density will (at most) show a ½ –order dependence. This aspect has not been previously fully appreciated.

For the HT mechanism, the exchange current density is dependent on the Heyrovsky rate constant, k_2^{eq}, and *B* (both directly, and through the dependence of $\theta_{H_{ad}}^{HT,eq}$ on B). Again there is no dependence of the reaction order on pH, and in this case the limiting values of the hydrogen reaction order are $^1/_2$ or 1. The difference between the hydrogen reaction order of the HT and TV mechanisms comes about because of the involvement of bimolecular hydrogen in the electrokinetic steps, c.f. Eq 31.

For the HTV mechanism, the exchange current density is associated with the sum of that associated with the TV and HT mechanisms. Hence, there is again no dependence of reaction order on pH. It is maybe surprising that the HTV mechanism shows no dependence on pH as the HV shows such a dependence. However, as is clear from the form of the exchange current density, it is the sum of two pH independent mechanisms, and hence is also pH independent. The limiting reaction order for hydrogen can take on three different values, 0, ½, and 1. As with the cases above, intermediate values are possible, but these are associated with a "transition region" where the reaction order is shifting between values.

3.5.2 Exchange current density from the slope of the micropolarisation region

Kinetic information for the hydrogen reaction is most frequently extracted from the micropolarisation region, as this allows the smallest perturbation to the system and hence leads to the least likelihood of introducing mass transport and Ohmic losses. The exchange current density is then extracted from the slope of the micropolarisation region under the assumption that the *hor*/*her* follow a Butler-Volmer type expression and that series expansion of the exponential function about η=0 is possible[19]:

$$j_{Spec}(\eta) = \left(\frac{2F}{RT} j_0\right)\eta \qquad \text{Eq 54}$$

where $j_{Spec}(\eta)$ is the experimentally measured specific current density at overpotential, η. Note that for thermodynamic reasons, the factor of two is required, as this allows a direct correspondence of the kinetic reaction with the Nernst equation at equilibrium (see Appendix A).

Table 3 provides the kinetic form of the slope of the micropolarisation region in terms of the individual kinetic parameters. Under certain conditions these slopes may simplify to the true exchange current density, although in

many cases they will not. We also provide the possible limiting reaction order for hydrogen which may be seen for the slope of the micropolarisation region. In all cases the reaction order for protons remain the same.

As we have the full mathematical form of the HV equation we have determined the mathematical form of this micropolarisation region by taking the derivative of Eq 17 (with $\theta_{H_{ad}}^{HV,eq}$ expanded by Eq 15) and setting η=0. This approach is preferable to taking the series expansion as it is more accurate.

$$\left(\frac{\partial j^{\mathrm{HV}}(\eta)}{\partial \eta}\right)_{\eta=0} = \frac{4\mathrm{F}^2}{RT}\frac{Kk_1^{\mathrm{eq}}k_2^{\mathrm{eq}}a_{\mathrm{H2}}}{(K+1)(Kk_1^{\mathrm{eq}}a_{\mathrm{H2}}+k_2^{\mathrm{eq}})} \qquad \text{Eq 55}$$

This further simplifies to

$$\left(\frac{\partial j^{\mathrm{HV}}(\eta)}{\partial \eta}\right)_{\eta=0} = \frac{4\mathrm{F}^2}{RT}\theta_{H_{ad}}^{HV,eq}\frac{k_2^{\mathrm{eq}}G}{(G+1)} = \left(\frac{\mathrm{F}}{RT}\right)F\theta_{H_{ad}}^{HV,eq}\left(\frac{1}{\frac{1}{4Kk_1^{\mathrm{eq}}a_{\mathrm{H2}}}+\frac{1}{4k_2^{\mathrm{eq}}}}\right) \qquad \text{Eq 56}$$

Hence the measured apparent "exchange current density" is really a composite of both electrochemical rate constants, and shows a complex dependence on hydrogen and hydrogen ion concentration. Rather than appearing as a parallel mechanism as it does in the true exchange current density, it appears as a serial mechanism

$$j_0^{app} = F\theta_{H_{ad}}^{HV,eq}\left(\frac{1}{\frac{1}{4Kk_1^{\mathrm{eq}}a_{\mathrm{H2}}}+\frac{1}{4k_2^{\mathrm{eq}}}}\right) \qquad \text{Eq 57}$$

$$j_{Spec}(\eta) = \left(\frac{F}{RT}j_0^{app}\right)\eta$$

Where $j_{Spec}(\eta)$ is the experimentally measured specific current density at overpotential, η. Note that in this case, the inclusion of the factor of 2 is not required as it is implicit in the derivation and leads to a consistent thermodynamic interpretation (see Appendix A). In general, the apparent exchange current density does not match the true exchange current density. However, there are two domains over which this equation simplifies into a form which approximates the true exchange current density depending on the relative magnitude of $Kk_1^{\mathrm{eq}}c_{\mathrm{H2}}$ and k_2^{eq}, or more succinctly by the magnitude of G. When G>>1, and the forward Heyrovsky reaction is much faster than the reverse Volmer reaction

$$j_{Spec}(\eta) = \left(\frac{F}{RT}j_0^{app}\right)\eta = \left(\frac{4F}{RT}j_0\right)\eta = \left(\frac{4F^2}{RT}\right)(\theta_{H_{ad}}^{HV,eq}k_2^{\mathrm{eq}})\eta \qquad if\ \mathrm{G} >> 1 \qquad \text{Eq 58}$$

It is interesting to note that the exchange current density do not exactly match, but instead there is a factor of four difference. Under these conditions, exchange current density will show zeroeth order dependence on hydrogen concentration and either first or zeroeth order dependence on hydrogen ion concentration depending on the magnitude of K through its effect on $\theta_{H_{ad}}^{HV,eq}$.

In comparison, when G<<1, which might be a more likely situation

$$j_{Spec}(\eta) = \left(\frac{F}{RT} j_0^{app}\right)\eta = \left(\frac{4F}{RT} j_0\right)\eta = \left(\frac{4F^2}{RT}\right)\left(\theta_{H_{ad}}^{HV,eq} K k_1^{\mathrm{eq}} a_{\mathrm{H2}}\right)\eta \qquad \text{Eq 59}$$

We have a reaction order of one for hydrogen and either zeroeth or 1st order reaction for proton activity depending on the magnitude of K.

For the TV reaction, determination of the effective exchange current density by differentiation of Eq 29 leads to a rather unwieldy expression, and so the exponential terms were first linearised by series expansion about η=0. This approach provides a good facsimile of the current density at close to the equilibrium potential. Differentiation of this function followed by setting η=0 provides the following

$$\left(\frac{\partial j^{\mathrm{TV}}(\eta)}{\partial \eta}\right)_{\eta=0} = \frac{4F k_2^{\mathrm{eq}} k_{\mathrm{ad}} k_{\mathrm{des}} a_{\mathrm{H2}} (1-\mathrm{B})}{(-a_{\mathrm{H2}} k_{\mathrm{ad}} + k_{\mathrm{des}})\left(4\mathrm{B} k_{\mathrm{des}} + k_2^{\mathrm{eq}} + \mathrm{B} k_2^{\mathrm{eq}}\right)} = \frac{4F\theta_{H_{ad}}^{TV,eq} k_2^{\mathrm{eq}} \mathrm{B}}{(Z + B(4+Z))} \qquad \text{Eq 60}$$

Further simplification provides, that for an experimentally measured specific current density at an overpotential, η,

$$j_{Spec}(\eta) = \left(\frac{F}{RT} j_0^{app}\right)\eta = \left(\frac{F}{RT} j_0\right)\eta = \left(\frac{4F^2}{RT}\right)\left(\frac{\theta_{H_{ad}}^{TV,eq} k_2^{\mathrm{eq}}}{\left(1 + \frac{Z}{4} + \frac{Z}{4B}\right)}\right)\eta \qquad \text{Eq 61}$$

We see that we can recover the "True" exchange current when both terms in Z in the denominator of Eq 61 tend to zero

$$j_{Spec}(\eta) = \left(\frac{F}{RT} j_0^{app}\right)\eta = \left(\frac{F}{RT} j_0\right)\eta = \left(\frac{4F^2}{RT}\right)\left(\theta_{H_{ad}}^{TV,eq} k_2^{\mathrm{eq}}\right)\eta \qquad if\ \left(\frac{Z}{4} + \frac{Z}{4B}\right) \to 0 \qquad \text{Eq 62}$$

This occurs when the Volmer reaction is slower than the H_{ads} recombination reaction and the rate of hydrogen adsorption is fast compared to desorption. If this is not the case then the exchange current density estimated from the micropolarisation region will be underestimated. As the micropolarisation region is affected by the rate of hydrogen adsorption/desorption, the possible reaction order for hydrogen changes to now also include the possibility of a value of unity. This higher value becomes possible when $\frac{Z}{4B} \gg 0$, i.e. when the Volmer step is faster than the hydrogen adsorption/desorption step. A situation which is commonly encountered on many metals.

The situation is similar for the HT mechanism. Series expansion about η=0 followed by setting η=0 provides an equation in which the denominator is modified from that seen for the true exchange current density, Table 3. In this case, the determination of the exchange current density from the linear polarisation region provides a valid value when

$$j_{Spec}(\eta) = \left(\frac{F}{RT} j_0\right)\eta = \left(\frac{4F^2}{RT}\right)\left(\frac{\theta_{H_{ad}}^{HT,eq} k_1^{eq} a_{H_2}}{\mathrm{B}}\right)\eta \qquad if\ \left(\frac{Y}{4B} + \frac{Y}{4B^2}\right) \to 0 \qquad \text{Eq 63}$$

That is, when the Heyrovsky step is much faster than both k_{ad} and k_{des}. As with the TV mechanisms, the number of limiting cases for hydrogen reaction order increases, although in this case the added possible value is a zeroth order dependence on hydrogen.

For the HTV equation, expansion about $\eta = 0$ and simplification provides an equation which is similar to the true exchange current density but is modified in both the numerator and denominator by the same factors seen for the TV and HT cases. It is only when both of these limitations are satisfied does the estimate of the exchange current density from the micropolarisation region converge to the true exchange current density

$$j_{Spec}(\eta) = \left(\frac{F}{RT} j_0\right)\eta = \left(\frac{4F^2}{RT}\right)\theta_{H_{ad}}^{HTV,eq}\left(\frac{k_1^{\mathrm{eq}} a_{\mathrm{H2}}}{B} + k_2^{\mathrm{eq}}\right) \qquad if\ \left(\frac{Y}{4B} + \frac{Y}{4B^2}\right) \to 0\ \boldsymbol{and}\ \left(\frac{Z}{4} + \frac{Z}{4B}\right) \to 0 \qquad \text{Eq 64}$$

That is, when both the Heyrovsky and Volmer kinetics are much faster than the chemical adsorption/desorption steps. Furthermore, if these cases are not satisfied, then an extra number of limiting reaction orders for hydrogen become possible including a negative reaction order, and a reaction order of $^3/_2$.

3.5.3 Exchange current density from back extrapolation of the log|j| vs η to the equilibrium potential

For the Butler-Volmer equation, the exchange current density calculated from extrapolation from large overpotentials is independent of the branch used, and matches the values determined from the micropolarisation region, but for the hydrogen reaction (and indeed any multi-step reaction), this may not be the case. The reason for this difference is that the reaction may be controlled by one slow step close to the equilibrium potential, but by another at large overpotentials. Back extrapolation assumes the slow step remains the same, but this may not be the case. Hence estimates of the "Exchange current density" via back-extrapolation of the current from large overpotentials to the equilibrium potential may lead to different values depending on whether the *her* or *hor* branches are used (e.g. see Figure 2(f) or Figure 5(f)), and hence it is necessary to individually solve for both branches. This approach is experimentally the most difficult to determine as it may involve operation in regions in which mass transport and Ohmic losses are large. Nonetheless, it is interesting to compare the results to the real exchange current density.

The dependence of current at large positive and negative overpotentials may be determined by substituting the limiting hydrogen coverage (Eq 16 for HV, Eq 45 for HTV, or 0 and 1 for the HT and TV equations, respectively) into the appropriate equation for current generation (Eq 17, Eq 29, Eq 39, or Eq 47). Back-extrapolation of these equations to the equilibrium potential provides a "limiting" exchange current, Table 3. For both the HV and HTV forms, the slope of the responses are $\frac{\beta RT}{F}$ and $\frac{-(1-\beta)RT}{F}$ (but cf below, other possible slopes are possible at intermediate potentials). For both the TV and HT, the slope is zero as the reaction is limited by the absorption/desorption chemical reaction at large overpotentials.

For the HV mechanism, the exchange current density calculated from the large overpotential extrapolation to the equilibrium potential are composed of the minimum and maximum hydrogen coverages (Eq 16) multiplied by one of the terms in the "true" exchange current density, Table 3. For the large positive extrapolation, the term is

associated with the Volmer step, as this will be the rds at large overpotentials. In comparison at large negative overpotentials, the term is associated with the reverse Heyrovsky step. It may be strange to see a term associated with the **forward** Heyrovsky step in the current associated with *her* region, but the conflict is resolved if one considers the equivalence shown in Eq 12, i.e. $k_{-1}^{eq} a_{H^+} = K k_1^{eq} a_{\mathrm{H2}}$. In order for the exchange current density calculated due to large overpotential extrapolation from each branch be the same, it is necessary that $\frac{k_{-1}^{eq} a_{H^+}}{\theta_{H_{ad}}^{\mathrm{HV}}(\eta \to -\infty)} = \frac{k_2^{eq}}{\theta_{H_{ad}}^{\mathrm{HV}}(\eta \to \infty)}$, where the denominators are taken from Eq 16. This is rather unlikely.

For both the TV and HT mechanisms the limiting current densities are associated with either the chemical adsorption step (large positive overpotentials) or desorption step (large negative overpotentials), Table 3. As with the HV case, it is unlikely that both $a_{\mathrm{H2}} k_{\mathrm{ad}}$ and k_{des} would have the same numerical value, and so it would be expected that the exchange current densities calculated from each approach would not be the same.

Finally, the HTV mechanisms shows extrapolated exchange currents similar to that seen for the HV mechanisms in which the equation is composed of the limiting hydrogen coverage (Eq 45) multiplied by one of the terms in the true exchange current density, Table 3. For the large positive overpotential this is associated with the Volmer step, and for the large negative overpotential this is associated with the Heyrovsky step. As with the HV equation above, it may be strange to see a term associated with the **forward** Heyrovsky step in the current associated with the *her* region, but the conflict is resolved if one considers the equivalence shown in Eq 42, i.e. $k_{-1}^{\mathrm{eq}} a_{H^+} = \frac{a_{\mathrm{H2}} k_1^{\mathrm{eq}}}{B}$, hence the relevance to the *her* is seen. As with the other cases above, it is unlikely that both branches would converge to the same exchange current density.

3.6 Estimation of "Tafel" slopes of log|j| vs η plots from experimental results

Significant care needs to be taken in reading too much into derived Tafel slopes, as in most cases a full Tafel slope does not develop and instead a "mixing" between different behaviours is seen. It is important to note that the potentials at which such behaviour occurs may be outside the region that can be experimentally accessed. Hence the validity (and usefulness) of the parameter may need to be questioned. Furthermore, as shown above, there may be intermediate regions with enhanced values of slope in the $log|j| vs\ \eta$ plots. In all cases these regions of enhanced slope may suggest much higher current densities at high overpotentials than those which can be achieved. The transition from one Tafel slope to another Tafel slope typically takes at least ~3 F/RT (~100mV at room temperature) and in order to develop a suitable and quantifiable slope, at least a further 3 F/RT is required. Identification of linear regions in the plots of $\log|j| \ vs\ \eta$ is facilitated by plots of $\frac{RT}{F} \frac{\partial log|j|}{\partial \eta}$ provided in the computable document format (CDF) files for each of the mechanisms examined, and available for download in supplementary material.

Depending on the mechanism used a variety of fully developed linear regions in the $\log|j| \ vs\ \eta$ plots are seen. A summary of the different values of the "measured" α values in terms of the mechanistic β value are provided in Table 3. The separation of terms is made easier by the cdf models provided with the paper, as it is possible to vary the value of β for a given set of parameters and see how this affects the value of α_{eff} seen in the plateau. It is

interesting to see that the full mechanistic derivation of the *hor/her* leads to distinct values of slopes with possible values of β, (1+β) and 2 for the anodic branch, and –(1-β), -(2-β) and -2 for the cathodic branch. Significant deviation of "Tafel slopes" away from the standard values of α and -(1-α) (i.e. values >1 for anodic, and <-1 for cathodic branches) have often in the past been interpreted as an increase of the number of electrons in the rate determining step[35]. However, in this case we see that enhanced values of "Tafel slope" develop naturally from the underlying analytical solutions to the kinetic equations. Examples for some of the enhanced slopes are illustrated in Figure 1-Figure 5.

3.7 Estimation of the free energy of adsorption of hydrogen on the electrode surface, $\Delta_{ads}G^{\ominus}_{H_2}$

Under equilibrium conditions the coverage of adsorbed hydrogen on the surface is in equilibrium with hydrogen in the adjacent solution phase

$$H_2 \rightleftharpoons 2H_{ads} \qquad \text{Eq 65}$$

As the derivation within this paper implicitly assumes a Langmuir adsorption isotherm, we have

$$\left(\frac{\theta_{H_{ad}}}{1-\theta_{H_{ad}}}\right) = a_{\mathrm{H2}}\, exp\left(\frac{-\Delta_{ads}G_{H_2,opd}}{RT}\right) \qquad \text{Eq 66}$$

Where $-\Delta_{ads}G_{H_2,opd}$ is the free energy of adsorption per mole of bimolecular hydrogen. At equilibrium, and under standard conditions, the hydrogen coverages take on their equilibrium values, and $a_{\mathrm{H2}} = 1$.

$$\left(\frac{\theta^{eq,\ominus}_{H_{ad}}}{1-\theta^{eq,\ominus}_{H_{ad}}}\right) = exp\left(\frac{-\Delta_{ads}G^{\ominus}_{H_2,opd}}{RT}\right) \qquad \text{Eq 67}$$

The LHS of this equation can be determined from the parameters $K^{\ominus}$ or $B^{\ominus}$ for the respective mechanisms. It is important to note that this free energy of adsorption is not the same as that associated with H_{upd} formed on some platinum group metals, as the mechanistic framework we have used in this paper does not include the presence of H_{upd}. Rather it is associated with the H_{opd} formed during the catalytic oxidation of H_2 or during the hydrogen evolution reaction[42-43].

4 Results and Discussion

In order to assess the different mechanisms towards the *hor/her* we have examined using the different models to fit experimental data using platinum as an electrode material. Although there is much work in the literature assessing the performance of platinum towards the *hor*/*her* it is now well recognised that mass transport masks the true activity of platinum for this reaction, and the measured "exchange current densities" are too low in many papers[8, 44]. This effect is illustrated in Figure 6 in which the *her/hor* polarisation plots are presented for a range of different electrochemical techniques transformed into specific activity (current density per real surface area). These techniques cover a wide range of mass transport regimes, in increasing order from microelectrodes with high surface area platinum catalyst (R_f=30) in contact with Nafion or acid[45], a 50 μm platinum microelectrode ($R_f \approx 1$) in contact

with aqueous acid, to a Pt rotating disk electrode disk (R_f ≈1, 7200 rpm) in contact with 0.1 mol dm^{-3} $HClO_4$[46], to a single platinum particle (450 nm in diameter) in acid[19] to results obtained utilising our floating electrode technique[16, 32] (R_f≈1) for an electrode in 1 mol dm^{-3} $HClO_4$. It is clear that there is a significant spread of results, but what is also clear is that mass transport effects occur even when the electrode is polarised at potentials at which the current is a small fraction of the mass transport limited current. This is shown in Figure 6(b) in which the current densities are transformed into "kinetic currents" utilising

$$j_k(\eta) = \left(\frac{j_{lim}\, j(\eta)}{j_{lim} - j(\eta)}\right) \qquad \text{Eq 68}$$

where the limiting currents are shown as dotted lines in Figure 6(a). Even after correction for the limiting currents the data do not converge to one plot, suggesting that Eq 68 is insufficient to correct for all mass transport effects. This is hardly surprising as the derivation of Eq 68 relies on the Butler-Volmer formalism, and the assumption that the mechanisms involves no adsorbed intermediates. It is only for the techniques which operate in the highest mass transport domains that there is any correspondence of the currents (i.e. floating electrode and 450 nm particle), suggesting that these techniques are operating close to the domain in which mass transport does not have too big an effect on electrokinetics. The other issue with mass transport corrections is that both the local limiting current density and the actual current density measured must be highly uniform across the entire surface and must be known to very high precision. For instance, in order to transform the rotating disk electrode data to that similar to the floating electrode data (a ca. 3 order of magnitude increase), the measured current density and limiting current density need to be measured at an accuracy better than 1 part in 10^4 and the current density (and limiting current density) needs to be uniformly distributed across the electrode to the same accuracy. This is virtually impossible to achieve, and no convincing RDE experiments have been performed to show that this is indeed the case.

More sophisticated correction of the electrokinetics for the hor/her has been attempted by including the variation of bimolecular hydrogen concentration at the electrode surface and using this to build a more accurate model of the perturbation of the electrokinetics by the mass transport effect[27, 38]. For metals on which the hydrogen reaction is facile (e.g. platinum group metals in acidic electrolytes), it is difficult to see how techniques such as the rotating disk electrode can be used due to the above mentioned requirements without going to exceptionally low loading (and in this case the mass transport regime becomes more complex)[8, 47], and hence it is necessary to use other techniques such as microelectrodes[19, 26, 38], SECM techniques[26, 48-50], or procedures which utilise gas phase transport of reactants[17-18, 32, 51]. For materials which show a much lower performance towards the *her/hor*, utilising techniques such as the RDE may be possible, but care must still be taken, especially in drawing conclusions about the activity of the catalyst, as the catalysts may be under a severe mass transport constraint.

In Figure 7 we present data for the *hor/her* for ultra-low loading electrodes composed of HiSpec 9100 60 % Pt/C catalysts using the newly developed vacuum filtration method to produce uniform dispersions of catalyst on a porous substrate and thus allow direct access of gaseous reactants/products to/from the catalyst surface. These electrodes are floated on the surface of an electrolyte with a structure which allows fast and facile access of

reactants, and for which we estimate a mass transport coefficient, k_{MT} > 10 cm s^{-1}. Further details on the fabrication of these electrodes and information about their performance is available in the experimental section and other publications[16-17, 32, 52]. In Figure 7(a) we show the performance in terms of specific activity (i.e. ratioed to the true surface area of the electrode as measured by upd hydrogen oxidation) of an electrode containing 2.2 μg_{Pt} cm^{-2} HiSpec 9100 60 % Pt/C electrode in 4 mol dm^{-3} $HClO_4$ as a function of temperature from 5°C to 60°C (278-333K). For comparison, the performance towards *hor/her* of a platinum rotating disk electrode (RDE) at 7000 rpm in a hydrogen saturated 0.1 mol dm^{-3} perchloric acid solution is also shown. The floating electrodes provide almost 1000-fold more current at the same potential when compared to the RDE due to the superior mass transport of the electrodes, and achieve specific current densities in excess of 1 A cm^{-2} at the highest temperature and at the peak activity point (i.e. a turnover frequency of >2000 hydrogen molecules per surface platinum site per second). Two peaks are seen in the response, and the performance decays at higher potentials. In a previous paper on hydrogen oxidation on individual supported platinum nanoparticles, a plateau was observed in the *hor* which varied in position and magnitude with platinum particle size[19]. This effect was interpreted and modelled as two different sites for the *hor* with different exchange current densities. Subsequently, other groups have interpreted the plateau in the *hor* as evidence of changeover from TV to the HV mechanism[27, 38], utilising the HTV mechanism to model this effect. However, the results in results in Figure 7 strongly support the presence of two different reaction sites as formation of such peaks is inconsistent with a mechanistic changeover from TV to HV, as in all cases these mechanisms show a monotonic increase in current density. Furthermore, there is a reduction in performance at higher overpotentials, and this is attributed to the effect of anion adsorption, which even for perchlorate, a weakly adsorbing anion, becomes appreciable under conditions of such high currents[16, 32]. It is interesting to also see that the *her* response on the RDE is much poorer than that of the floating electrode, suggesting that the mass transport plays an important for the *her* too. Figure 7(b) shows the response of an electrode in 0.5 mol dm^{-3} perchloric acid as function of hydrogen partial pressure from 0.029 to 0.126 bar hydrogen (balance nitrogen). Even at the lowest partial pressure, the performance is greater than the RDE. Figure 7(c) shows both sets of data presented on a logarithmic current scale. It is interesting to note that at high potentials, the current decays away much quicker and follows an exponential decay. This faster roll off in current starts at 0.70V and hence is assumed to be associated with the formation of OH_{ad} on the platinum surface which starts at this potential.

4.1 Fitting of data

In a previous paper, we fit the response of a large set of data from similar electrodes to the HV mechanism over the micropolarisation region from -10 to 10 mV utilising the linear form of the HV equation at the equilibrium potential, Eq 56, and found a good correspondence to the data[32]. In the following section, we use the full HV, TV, and HTV models to fit the *hor/her* response over a much wider potential range in order to assess which model is the most appropriate to replicate our data. As our data is to all intents mass transport free, we can use the models we have developed above without having to introduce added complications due to mass transport effects as is required when trying to assess RDE data[27, 38]. Furthermore we fit our data as a function of pH, hydrogen partial pressure, and

temperature, a much wider parameter space than typically used for these sorts of studies, which typically rely on rather small datasets.

In our model derivations, we have for simplicity assumed that the number of available sites for adsorption is (1-$\theta_{H_{ad}}(\eta)$). In fact, as we discussed above, the situation is somewhat more complicated and that the number of available sites for adsorption, especially at higher potentials may be much less than this term suggests. A more accurate approach may be to write this term as (1-$\theta_{Spectator}(\eta) - \theta_{H_{ad}}(\eta)$) where the extra term is associated with the species that adsorb more strongly than the hydrogen on the surface. As we have determined that the PZTC for these catalysts is 0.24 ± 0.01 V vs. RHE[32], and that the decay in current is correlated with anion adsorption, we only fit over a potential region much less than this value so that anion adsorption occurs to a very limited extent. A more sophisticated model would deal with such blocking species on the surface. We also only consider a single surface which leads to a single set of parameters. Within our model, a_{H_2} is the activity of dissolved hydrogen and equivalent to the change in partial pressure of hydrogen, P_{H_2}, assuming Henry's Law

$$a_{H_2} = a_{H_2}^{\ominus}\left(\frac{P_{H_2}}{P_{H_2}^{\ominus}}\right) \cong \frac{c_{H_2}}{c_{H_2}^{\ominus}}\left(\frac{P_{H_2}}{P_{H_2}^{\ominus}}\right) \quad \text{Eq 69}$$

Where $a_{H_2}^{\ominus}$ and $P_{H_2}^{\ominus}$ are the standard state activities of hydrogen in solution and in the gas phase (i.e. $P_{H_2}^{\ominus}$ = 1 bar, $a_{H_2}^{\ominus} = 1$). $c_{H_2}^{\ominus}$ is the saturated concentration of hydrogen in the ionomer phase immediately adjacent to the catalyst particle in equilibrium with 1 bar H_2 gas, and is taken as being 5.10×10^{-7} mol cm^{-3} [45].

Each of the microscopic steps may be associated with their own activation energy

$$k_1^{\mathrm{eq}}(T) = k_1^{\mathrm{eq,STP}} e^{-E_{a,1}/R\left({}^1/_T - {}^1/_{298.15}\right)} \quad \text{Eq 70}$$
$$k_2^{\mathrm{eq}}(T) = k_2^{\mathrm{eq,STP}} e^{-E_{a,2}/R\left({}^1/_T - {}^1/_{298.15}\right)}$$
$$k_{ad}(T) = k_{ad}^{\mathrm{STP}} e^{-E_{a,ad}/R\left({}^1/_T - {}^1/_{298.15}\right)}$$

although in order to reduce complexity we make the assumption that the reaction appears to be controlled by a single activation energy, and as such we can write

$$j_T(\eta) = j_{STP}(\eta) e^{-E_a/R\left({}^1/_T - {}^1/_{298.15}\right)} \quad \text{Eq 71}$$

In performing the fitting procedure we fit all data sets simultaneously (i.e. 13 datasets comprising seven hydrogen partial pressures and six different temperatures) using the same set of parameters. This approach is preferable to fitting each dataset individually (which would give the appearance of much better fits, as each trace would have an optimised set of parameters), but which would not constrain the solution to values which optimised the fit across the entire dataset – i.e. we sacrifice getting the best possible fit for each experimental curve by having a more general and applicable solution. The partial pressure of hydrogen was corrected for the vapour pressure of water, which especially at higher temperature can lead to significant variation. Some extra comments associated with fitting are listed in Appendix B.

4.2 Fitting data to the Heyrovsky-Volmer mechanism

For the TV reaction, we fit five parameters $k_2^{\ominus}$, $K^{\ominus}$, $G^{\ominus}$, E_a, and β to Eq 19 modified by Eq 71. Although Eq 19 contains no explicit dependence on a_{H_2} and a_{H^+}, these parameters enter into the equations through the definition of *G* and *K* respectively to give a specific value of G^{eq}, and K^{eq} for each experimental condition ($K^{eq} = K^{\ominus}/a_{H^+}$, $G^{eq} = G^{\ominus}a_{H_2}/a_{H^+}$). Likewise, $k_2^{\ominus}$ is automatically determined as all data sets are measured vs RHE for the appropriate a_{H_2} and a_{H^+} used. Hence the five parameters are used to simultaneously fit all 13 datasets. The fit was performed over the potential range -50 to +50 mV.

We have previously used the linear approximation about the equilibrium potential to fit the data over the potential range -10mV to 10mV. Using the full HV equation, we find that we can extend the range of suitable fit to -50mV..+50 mV. Beyond this range, especially at positive overpotentials we find that the fits diverge. At positive overpotentials our HV model over-predicts the current as it does not include the effect of the reaction shutting down due to anion adsorption. A comparison between the fit results (broken lines) and data (points) is provided in Figure 8a. The fitting parameters used to provide the best fit to the data sets are provided in Table 4, along with a number of parameters derived from those values. At higher temperatures and increased hydrogen partial pressures the fit remains relatively good, with greater deviation seen at the lower hydrogen partial pressures. A β value of 1/3 is determined from the fitting process, which is somewhat lower than the usual value of ½ ascribed to the hydrogen reaction. An activation energy of 18 kJ mol^{-1} is determined through the fitting procedure – this is the same as the experimentally observed activation energy in our previous paper[32], although a little higher than the value determined during the fitting of results (15.5 kJ mol^{-1}) in that paper. In our previous paper we used a data set which straddled a wider range of pH values, as the HV mechanism is the only one to show an effect on the exchange current density due to pH beyond the shift in equilibrium potential, whereas neither the TV nor the HTV mechanisms show a variation in kinetics beyond that associated with the shift in equilibrium potential (i.e. the exchange current density for both of these reactions is pH independent). The value of $K^{\ominus}$ determined from the fitting data is 3.09, which is in good agreement with the value of $K^{\ominus}$ determined in our previous paper of 2.6, suggesting that under standard conditions, the forward Volmer reaction is somewhat faster than the reverse Volmer reaction The values of $K^{\ominus}$ and $G^{\ominus}$ which we determine from our data provide values of $k_1^{\ominus}$ and $k_2^{\ominus}$ of 8.6×10^{-7} and 5.1×10^{-6} $\mathrm{mol\ cm^{-2}s^{-1}}$. These values are half and 4-5 times larger than the values determined using the cruder fit of the linear potential region (1.79×10^{-6} and 1.19×10^{-6} $\mathrm{mol\ cm^{-2}s^{-1}}$). The difference is probably associated with the previous approach assuming a value of β of 1/2, whereas in this case β was used as a fitting coefficient. Using the $k_1^{\ominus}$ and the saturated hydrogen concentration (5.1×10^{-7} $\mathrm{mol\ cm^{-3}}$ from ref[45]), a value of 1.7 cm s^{-1} is calculated.

It is salient to consider what these parameters mean in terms of simplification of the *hor/her* to a Butler-Volmer type formalism as described in Eq 20 and Eq 21. Neither the requirement that $K^{\ominus} \cong 1$, nor that $G^{\ominus} \ll 1$ is met, suggesting that such a model is poor at describing the hydrogen reaction. Comparison of model curves generated using Eq 19 and Eq 20 using the parameters in Table 4 shows that there is almost a 20% error across the entire potential range studied in Eq 20 over the more correct Eq 19.

The hydrogen coverage values determined from the fitting parameters show that at the equilibrium potential under standard conditions, the hydrogen coverage is 0.24, and this increases to a maximum value of 0.38 at large negative overpotentials. Utilising Eq 67 and the equilibibrium hydrogen concentration under standard conditions a value of $\Delta_{ads}G^{\ominus}_{H_2,opd}$ of +2.8kJ mol^{-1} is calculated, a value very close to the value of zero predicted on the basis of platinum's performance close to the apex of the volcano plot of activity for the hydrogen reaction[43, 53]. The equilibrium hydrogen coverage is fairly similar to the value of 0.179 determined on an Pt rotating disk electrode by Rau et al[29]. At large positive overpotentials the coverage has a non-zero value of 0.14. The true exchange current density is 183 mA cm^{-2} under standard conditions. This value is about 10% larger than the value determined solely from the micropolarisation region. In comparison there is a much larger difference with exchange current densities determined by extrapolating the large overpotential response back to the equilibrium potential which straddle the true exchange current density and over and underestimate it by about 20% and 10% respectively. The sensitivity of the exchange current density to pH changes i.e. $\left(\frac{\partial \log_{10}(j_0)}{\partial \log_{10}(a_{H^+})}\right)_{STP}$ is 0.41, close to the value of 0.38 determined in our previous paper when fitting the micropolarisation region[32]. As in that paper, the mechanism appears to be in transition from a reaction of one to zero as pH decreases. We calculate that the effect this parameter has on the exchange current is to increase the value from 0.14 A cm^{-2} to 0.314 A cm^{-2} as the acid strength is changed from 0.5 to 4 mol dm^{-3} $HClO_4$.

We have taken the parameters determined from the fitting procedure and generated a plot for the *hor*/*her* over a moderate potential range in order to more fruitfully understand what the model potentially tells us about the reaction, Figure 9(a). In this figure we also plot the currents associated with each step of the reaction (Forward/Reverse Heyrovsky and Forward/Reverse Volmer), and also plot the different exchange current densities along with extrapolation of the current at large overpotentials back to the equilibrium potentials. For comparison, in the bottom part of Figure 9(a) we also plot $\theta^{\mathrm{HV}}_{H_{ad}}$ and the effective Tafel slope ($\frac{2.303\,RT}{\beta F}$, $\frac{-2.303\,RT}{(1-\beta)F}$) utilising the β value determined from the fit. The results show a slight asymmetry in the electrokinetic response in that the *her* is more facile than the *hor*, and as a result the exchange density extrapolated from the large negative overpotential region is larger than that from the large overpotential region. It is seen that a linear region in the log(j) vs η plot is only seen when $|\eta|$ >150 mV. This suggests that experimental data which shows linear "Tafel regions" at lower overpotentials may be due to artefacts. At these larger overpotentials, the slope of the Tafel plots are well described by the β-value used within the electrokinetic model.

4.3 Fitting data to the Tafel-Volmer mechanism

For the TV reaction, we fit five parameters: $k^{\ominus}_{des}$, $B^{\ominus}$, $Z^{\ominus}$, E_a, and β to Eq 30 modified by Eq 71. For each set of data, a_{H_2} enters into the equations through $B^{\ominus}$ to give a specific value of B^{eq}. Hence the five parameters are used to simultaneously fit all 13 datasets. The fit was performed over an extended range compared to that used for the HV fit: -50 to +100 mV.

The fit of the TV equation to the data set is good, especially for the results at lower hydrogen partial pressure, Figure 8(b), accurately tracking the performance for both the *her* and *hor*. The presence of a peak is accurately captured by assuming a rate limiting hydrogen adsorption step (see below). For the higher partial pressure results, and especially at higher temperatures, there is a tendency to underestimate the current at higher overpotentials. This might be associated with hydrogen adsorption step having a lower activation energy than the "global" activation energy used, and hence this aspect is not adequately captured. Alternatively, as the exchange current density of the TV mechanism is not pH sensitive, the change in pH of the electrolyte might be having an effect on the reaction which is not captured by the TV mechanism, although as was seen in the HV mechanism, the ca 2-fold increase in going from 0.5 to 4 mol dm^{-3} $HClO_4$ might be important in obtaining good fits. Nonetheless, the *her* currents are adequately captured by the fits.

The fit parameters determined during the fit procedure are displayed in Table 4, along with a number of parameters derived from those values. The fitted value of the molecular symmetry factor, β, is close to ½. The reaction order with respect to bimolecular hydrogen under equilibrium conditions and at STP, i.e. $\left(\frac{\partial \log_{10}(j_0)}{\partial \log_{10}(a_{H_2})}\right)_{STP}$, is 0.39. Somewhat less than the limiting value of ½, showing that the mechanism is in a transition region where $B^{\ominus} \approx 1$. The value of the equilibrium hydrogen coverage under standard conditions, $\theta_{H_{ad}}^{\ominus}$, is 0.22, close to the value determined for the HV mechanism. This value corresponds to a value of $\Delta_{ads}G_{H_2}^{\ominus}$ of 3.1 kJ mol^{-1}, about 10% higher than the value determined for the HV mechanism, but still very close to zero. The value of $k_{des}^{\ominus}$ determined from the fitting procedure is 2.1×10^{-5} mol cm^{-2} s^{-1}. This value is about 10 times greater than the value of $k_{ad}^{\ominus}$ determined from the fitting parameters suggesting that under standard conditions, the hydrogen recombination process on platinum is about 10 times faster than the adsorption process. The value of $k_{ad}^{\ominus}$ determined, combined with the saturated hydrogen concentration provides a value of 3.4 cm s^{-1}. This is close to the value determined by Vogel *et al* of 2.4 cm s^{-1} determined at 295 K using low-pressure gas phase H_2/D_2 exchange over platinum[15]. The true exchange current density under standard conditions is 189 mA cm^{-2}, very close to the value determined for the HV mechanism. The exchange current determined from the micropolarisation region is 129 mA cm^{-2}, meaning that attempts to measure the exchange current density using the micropolarisation region would underestimate the true value by about 30%, demonstrating the appreciable effect of the extra terms in the denominator of Eq 61 (i.e. $\left(\frac{Z}{4}+\frac{Z}{4B}\right) = 0.47$ using the fitting parameters). The limiting currents associated with hydrogen adsorption and desorption, are 329 and 4060 mA cm^{-2}, and these values put a limit on the ultimate performance of the *hor/her* assuming the mechanism is a TV one. The activation energy determined form the data is 23 kJ mol^{-1}, a little larger although similar in value to that determined from fitting the HV mechanism.

As was performed for the HV mechanism, we have taken the parameters determined from the fitting procedure and generated a plot for the *hor*/*her* over a moderate potential range in order to more fruitfully understand what the model potentially tells us about the reaction, Figure 9(b). The limiting current on the *her* can be seen as occurring

once the overpotential reaches ca -300mV, and the different exchange current densities are plotted showing the wide divergence depending on the method used to measure them. No clear Tafel slope is seen in the plot.

4.4 Fitting data to the HTV mechanism

For the HTV mechanism, we fit six parameters: $k_{des}^{\ominus}$, $B^{\ominus}$, $Y^{\ominus}$, $Z^{\ominus}$, E_a, and β to Eq 47 modified by Eq 71. For each set of data, a_{H_2} enters into the equations through $B^{\ominus}$ and $Y^{\ominus}$ to give a specific value of B^{eq} and Y^{eq}. The fit was performed over the same range as for the TV fit, i.e. -50 to +100 mV.

The fit of the HTV equation to the data set is good, although not appreciably better than that achieved using the TV equation at the expense of one more fitting parameter. There is a good fit especially for the lower hydrogen partial pressures, Figure 8(c), accurately tracking the performance for both the *her* and *hor*, although as with the HV mechanism, there is a divergence of fits at larger potentials due to the electrochemical reaction out running the chemical Tafel step.

The fit parameters determined during the fit procedure are displayed in Table 4, along with a number of parameters derived from those values. The fitted value of the molecular symmetry factor, β, is 0.71 suggesting a transition state which favours the products. The value of $B^{\ominus}$ is very similar to that found for the TV mechanism. This parameter leads to an equilibrium hydrogen coverage and value of $\Delta_{ads}G_{H_2}^{\ominus}$ which are close to the values seen for both the HV and TV mechanisms. The value of $k_{des}^{\ominus}$, one of the other fitting parameters is also close to that seen for the TV mechanism, differing by less than a factor of two. The value of $k_{ad}^{\ominus}$ determined from this parameter, 2.1 cm s^{-1} is very close to that given by Vogel *et al* of 2.4 cm s^{-1} as discussed above[15]. The $Z^{\ominus}$ parameter (associated with the Volmer step) is about three times larger than the same parameter for the TV mechanism, and this then leads to a value $k_2^{\ominus}$ which is within 50% of the value determined for the TV mechanism. The calculated activation energy, 20 kJ mol^{-1} is intermediate between the values obtained for the HV and TV mechanisms. The kinetic constant associated with the forward Heyrovsky step, $k_1^{\ominus}$, is ten times smaller than the value for the HV mechanism. The requirement for a small value for this parameter is associated with the deviation of current at large positive overpotentials. The similarity of parameters between the HTV and the TV mechanism is not so surprising as the same fundamental processes are at work.

Figure 9(c) shows the breakdown of the electrochemical currents into the separate forward/reverse Heyrovsky/Volmer part currents which sum to the total electrochemical current. It can be seen that close to the equilibrium potential, the Volmer currents are enhanced due to the extra current associated with the Tafel step. As the applied potential moves away from the equilibrium potential, the relative magnitude of the Tafel step becomes small relative to the Heyrovsky step. This point is emphasized in Figure 9(d) derived using Eq 51, Eq 52, and Eq 53. It can be seen that close to the equilibrium potential, the majority of the current is derived from the TV mechanism, whereas further way there is an increase in the HV mechanism. There is no contribution of the HT mechanism at any potential studied. Furthermore, the ratio of current from each mechanism is not symmetric about the equilibrium potential, rather it is stretched on the *her* side. This can be also seen in the form of the current response in Figure

9(c) in which a there is a small plateau on the *hor* side close to the equilibrium potential, but a much wider deviation on the *her* side. Indeed, even at -300 mV overpotential, there is still a significant contribution of the TV mechanism to the current whereas by 200mV overpotential, virtually all the current comes from the HV mechanism. This effect also has a significant impact on the exchange current densities, Table 4. The "True" exchange current density is dominated by the TV mechanism, and is significantly higher than the exchange current density determined for the HV and TV mechanisms. Furthermore, it is about two-fold greater than the value determined from the linear region about the equilibrium potential (whose value is similar to that determined for the HV and TV mechanisms), this comes about as the $\left(\frac{Z}{4}+\frac{Z}{4B}\right)$ term in Eq 64 is significantly greater than zero. Rather surprisingly, the exchange current densities associated with the large overpotential extrapolation are very small in contrast to the true exchange current density – only 5% and 14% of the true exchange current density. This is because the *hor/her* "overperforms" in the region close to the equilibrium potential due to the fast TV reaction, which more than compensates for the slow HV mechanism. The scatter of the exchange current densities is easily seen in Figure 9(c). The Tafel slope associated with the *hor* only develops at large ovepotentials (>200mV), although there is a peak at lower potentials. Measurements made in this intermediate regime, and utilising only a small range of data may interpret these measurements as implying a spuriously large "Tafel Slope". In reality, this is associated with the details of the electrokinetics and a changeover from one mechanism to another. The effect is even more extreme on the *her* side where the "Tafel slope" remains far away from the expected one on the basis of β, even at -300 mV. The reaction order with respect to bimolecular hydrogen under equilibrium conditions and at STP, i.e. $\left(\frac{\partial \log_{10}(j_0)}{\partial \log_{10}(a_{H_2})}\right)_{STP}$, is 0.39 which is the same as the value determined for the TV mechanism.

5 Conclusion

We have developed and applied to experimental data a new theoretical framework for examining the *hor/her*. This approach allows formulation of a simplified electrokinetic framework which allows determination of reaction orders and Tafel slopes for different sets of kinetic parameters, and hence aids identification of appropriate mechanisms. It is interesting to note that only the Heyrovsky-Volmer mechanisms shows an exchange current which will change with pH, whereas in all other cases the exchange current should be pH independent (at least within the pH range in which the mechanisms listed in Eq 1 to Eq 6 operate). Similarly, the limiting reaction order dependence of the exchange current density on bimolecular Hydrogen shows possible values of 0, ½ and 1 depending on the mechanisms and precise values of the appropriate parameters.

Within this paper we have shown that the standard approach of assuming that we can treat multi-step reactions in the same way as the Butler-Volmer equation is a very poor choice. Although for the *her/hor* there are individual cases where particular combinations of parameter allow such a simplification, this is not guaranteed. Hence some conclusions derived from such a simplification may be ill-judged.

From both the "atlas" of possible response and the specific fitting results for *hor/her* on Pt/C in acid, it can be seen that a consistent slope in the Log(j) vs η plot is only seen for $|\eta|$>>100 mV. This suggests a significant limitation on

the ability to see such slopes in experimental data for the *hor/her*, as it can be difficult to operate at such large overpotentials without incurring significant mass transport losses using, for instance, the rotating disk electrode. Furthermore, the concept of using an exchange current density and "Tafel slope" is somewhat devalued as an approach to extrapolate performance, as it is seen that there appears to always be a transition of mechanism close to the equilibrium potential, and the transition between mechanisms requires at least 100mV of overpotential.

Fitting a set of experimental data to the HV, TV and HTV mechanisms for data for platinum gives close agreement to some parameters. For instance the equilibrium hydrogen converage for all mechanisms, $\theta_{H_{ad}}^{\ominus}$, is between 0.22-0.24, implying a value of $\Delta_{ads}G_{H_2,opd}$ close to +3 kJ mol^{-1}, close to the value of zero expected for Pt. Likewise the activation energy for the *her/hor* is found to be between 18-23 kJ mol^{-1}. Although there is a 10-fold variation in the value of the Heyrovsky reaction kinetic constant, $k_1^{\ominus}$, between the HV and HTV mechanisms. Across all mechanisms, the Volmer rate constant, $k_2^{\ominus}$, shows a relatively small deviation. The Volmer rate constant is consistently faster than the Heyrovsky rate constant, in agreement with previous literature suggesting that the Volmer step is fast. There is good agreement for the values of the chemical hydrogen steps associated with adsorption and desorption, $k_{ad}^{\ominus}$ and $k_{des}^{\ominus}$.

It is worthwhile considering which of the mechanisms is best suited to represent the experimental data, and this gives rise to a conundrum. It is difficult to imagine an HV mechanism which is able to accurately replicate the data in Figure 7, especially at high potentials where the experimental data shows that the reaction appears to shut down. At such high overpotentials, the only way that an HV mechanism could achieve such low currents would be if the surface was highly blocked. This would require a blocking layer on the surface which is highly efficient and which would be also expected to severely limit the oxygen reduction reaction, something which is known not to occur on these electodes[52]. An intriguing alternative would be if the entropic barrier suggested by Rossmeisl et al[11] acts to shut down the reaction at large overpotentials. In contrast, the TV mechanism would offer suitable advantages in this aspect, as the maximum rate of *hor/her* is limited by the chemical adsorption/desorption steps[15] (as for instance performed in [29] where an HTV mechanism is used but with a Heyrovsky step which is 5 orders of magnitude lower than the Tafel step). But the TV or HTV mechanisms do not show a dependence of the exchange current density with pH, something which occurs within the experimental data.

The assumption in this paper is that underpotential deposited hydrogen (H_{upd}), commonly formed on many platinum group metals, does not take part in the reactions is common to the approach taken by a number of others[27, 29, 54], although we have previously developed a model which explicitly includes H_{upd} as an intermediate[19]. In reality, the true situation is probably intermediate between these two extremes. A future modification to this model should try to incorporate that aspect and also deal with the shutdown of the *hor* at higher potentials due to anion adsorption.

6 Acknowledgements

The authors would like to thank the U.K. Engineering and Physical Sciences Research Council (EPSRC) for funding through Hydrogen to Fuel Cells (H2FC SUPERGEN) Flexible Funding Award EPSRC Grant Ref. EP/J016454/1; and

EP/M023508/1 “Innovative concepts from Electrodes to Stacks”. They would also like to thank Dr Matthew Markiewicz for helpful comments during the preparation of the manuscript. The data used for generating the experimental plots, and spreadsheets which allow fitting of data to each of the mechanisms are available for download, as are the computable document format examples of the different mechanisms[34].

7 Appendix A

The Nernst equation for the hydrogen reaction is

$$E^{eq} = E^{\ominus} + \left(\frac{RT}{2F}\right) log_e\left(\frac{{a_{H^+}}^2}{a_{H_2}}\right) \qquad E^{\ominus} = 0 \qquad \text{Eq 72}$$

As we are dealing with a multistep reaction, which involves a surface adsorbed intermediate (H_{ad}), we require that the intermediate reactions also fulfil the above criteria for the equilibrium potential. Under standard conditions we can write for the HV mechanism the two individual ratios of reactants to products for the Heyrovsky and Volmer steps (the same approach is applicable to the other mechanisms) and the coverage terms in H_{ad} cancel

$$E^{eq} = E^{\ominus} + \left(\frac{RT}{2F}\right) log_e\left(\frac{a_{H^+}\theta_{H_{ad}}^{eq}}{a_{H_2}\left(1-\theta_{H_{ad}}^{eq}\right)} \frac{a_{H^+}\left(1-\theta_{H_{ad}}^{eq}\right)}{\theta_{H_{ad}}^{eq}}\right) \qquad \text{Eq 73}$$

At any reversible potential, the net reaction must be zero so

$$k_1^{eq} a_{H_2}\left(1-\theta_{H_{ad}}^{eq}\right) - k_{-1}^{eq} a_{H^+}\theta_{H_{ad}}^{eq} + k_2^{eq}\theta_{H_{ad}}^{eq} - k_{-2}^{eq} a_{H^+}\left(1-\theta_{H_{ad}}^{eq}\right) = 0$$
$$\frac{k_1^{eq} a_{H_2}\left(1-\theta_{H_{ad}}^{eq}\right) + k_2^{eq}\theta_{H_{ad}}^{eq}}{k_{-1}^{eq} a_{H^+}\theta_{H_{ad}}^{eq} + k_{-2}^{eq} a_{H^+}\left(1-\theta_{H_{ad}}^{eq}\right)} = 1 \qquad \text{Eq 74}$$

Furthermore, there is the requirement that the hydrogen coverage is also stationary, and so

$$k_1^{eq} a_{H_2}\left(1-\theta_{H_{ad}}^{eq}\right) + k_{-2}^{eq} a_{H^+}\left(1-\theta_{H_{ad}}^{eq}\right) - k_{-1}^{eq} a_{H^+}\theta_{H_{ad}}^{eq} - k_2^{eq}\theta_{H_{ad}}^{eq} = 0$$
$$\frac{k_1^{eq} a_{H_2}\left(1-\theta_{H_{ad}}^{eq}\right) + k_{-2}^{eq} a_{H^+}\left(1-\theta_{H_{ad}}^{eq}\right)}{k_{-1}^{eq} a_{H^+}\theta_{H_{ad}}^{eq} + k_2^{eq}\theta_{H_{ad}}^{eq}} = 1 \qquad \text{Eq 75}$$

The constraints introduced by Eq 74 and Eq 75 can only be satisfied when

$$k_1^{eq} a_{H_2}\left(1-\theta_{H_{ad}}^{eq}\right) = k_{-1}^{eq} a_{H^+}\theta_{H_{ad}}^{eq}$$
$$k_2^{eq}\theta_{H_{ad}}^{eq} = k_{-2}^{eq} a_{H^+}\left(1-\theta_{H_{ad}}^{eq}\right) \qquad \text{Eq 76}$$

and thus

$$\frac{k_1^{eq} a_{H_2}}{k_{-1}^{eq} a_{H^+}} = \frac{\theta_{H_{ad}}^{eq}}{\left(1-\theta_{H_{ad}}^{eq}\right)} \qquad \text{Eq 77}$$

and

$$\frac{k_2^{eq}}{k_{-2}^{eq} a_{H^+}} = \frac{\left(1-\theta_{H_{ad}}^{eq}\right)}{\theta_{H_{ad}}^{eq}} \qquad \text{Eq 78}$$

Substituting Eq 77 into Eq 78 provides

$$\frac{(a_{H^+})^2}{a_{H_2}} = \frac{k_{-1}^{eq} k_{-2}^{eq}}{k_1^{eq} k_2^{eq}} \qquad \text{Eq 79}$$

At the equilibrium potential, when the activity of reactants are one

$$\frac{k_1^{\ominus} k_2^{\ominus}}{k_{-1}^{\ominus} k_{-2}^{\ominus}} = 1 \qquad \text{Eq 80}$$

This equation then also feeds into the constraint on the value of the rate constants, Eq 11. As the Nernst equation applies, we can satisfy the thermodynamic requirements of Eq 79 and Eq 80 via

$$\begin{aligned} k_1^{eq} &= k_1^{\ominus} e^{\beta f (E^{eq} - E^{\ominus})} \\ k_2^{eq} &= k_2^{\ominus} e^{\beta f (E^{eq} - E^{\ominus})} \\ k_{-1}^{eq} &= k_{-1}^{\ominus} e^{-(1-\beta) f (E^{eq} - E^{\ominus})} \\ k_{-2}^{eq} &= k_{-2}^{\ominus} e^{-(1-\beta) f (E^{eq} - E^{\ominus})} \end{aligned} \qquad \text{Eq 81}$$

$$f = \frac{\mathrm{F}}{RT}$$

Such an approach applies equally well to the other mechanisms studied.

8 Appendix B

During the fitting of the data, a large range of parameters were tried as initial guesses in order to assure suitable convergence. During this process, it was found that there was a family of fitting parameters which specified a class of curves which reasonably well matched the data (although not as well as the ultimate fit) when β was fixed at 1/2. For these fits, although some parameters were fixed, others could be varied, with one of the other parameters changing in opposition to give the same goodness of fit. Such a relationship implies that the equations listed within this paper may be simplified to less complex forms over some range of parameters (indeed, such a simplification is what underlies Eq 20 and Eq 21). In all of these cases it was observed that although there were differences in the IV curves that were created with those parameters, those differences only occurred at overpotentials well beyond what was experimentally accessible – hence they did not contribute to the "goodness of fit".

For the HV fit, the "approximately optimum" solution was found over a range of $k_2^{\ominus}$ from 3×10^{-6} to 1000 mol cm^{-2} s^{-1}. Over this range of values for $k_2^{\ominus}$, $k_1^{\ominus}$ was always fixed at 7.0×10^{-7} mol cm^{-2} s^{-1} and $K^{\ominus}$ was always fixed at 5.4. This relationship makes sense as it implies that forward Volmer always needs to be faster than the forward Heyrovsky. Hence $k_1^{\ominus}$ can be accurately determined from these fits, as can $K^{\ominus}$ (the ration between $\frac{k_2^{eq}}{k_{-2}^{eq}}$), but $k_2^{\ominus}$ is rather poorly defined.

For the TV fit, there is a similar situation. For all the "approximately optimum" solutions, $k_{ad}^{\ominus}$ does not vary at all (2.3×10^{-6} mol cm^{-2} s^{-1}), as this parameter is required to produce a limitation, or "peak" in the *hor*. In contrast, as no limitation in the *her* is seen, there are a wide range of values of $k_{des}^{\ominus}$ that satisfy the fit. In principle any value of $k_{des}^{\ominus}$ greater than 10^{-4} mol cm^{-2} s^{-1} will not cause deviation to the *her* curve (for values smaller than this, a plateau will start to form at overpotentials close to those that were measured). Within this domain, it is found that the ratio of $Z^{\ominus}/B^{\ominus}$ is constant at 1.37 (close to the ratio of the best fit values of 1.5).

For the fitting of the HTV data, the situation is similar to both cases mentioned above. Both $k_{ad}^{\ominus}$ (1.0×10^{-6} mol cm^{-2} s^{-1}) and $k_1^{\ominus}$ (1.9×10^{-7} mol cm^{-2} s^{-1}), are constant over all "approximately optimum" solutions whereas $k_{des}^{\ominus}$ can take on

values >10^{-6} mol cm^{-2} s^{-1} and $k_2^{\ominus}$ shows values between 10^{-2}-10^{-5} mol cm^{-2} s^{-1}. The best fit values of these parameters lie in these ranges.

Table 2 Comparison of different equations to model the *her/hor* for the Heyrovsky-Volmer (HV), Tafel-Volmer (TV), Heyrovsky-Tafel (HT) and Heyrovsky-Tafel-Volmer (HTV) reactions.

Mech.	$\frac{d\theta_{H_{ad}}}{dt}$	j/F	Parameters	Derived Parameters
HV	$k_1 a_{H_2}(1-\theta_{H_{ad}}^{HV}) - k_{-1} a_{H^+} \theta_{H_{ad}}^{HV} - k_2 \theta_{H_{ad}}^{HV} + k_{-2} a_{H^+}(1-\theta_{H_{ad}}^{HV})$	$k_1 a_{H_2}(1-\theta_{H_{ad}}^{HV}) - k_{-1} a_{H^+} \theta_{H_{ad}}^{HV} + k_2 \theta_{H_{ad}}^{HV} - k_{-2} a_{H^+}(1-\theta_{H_{ad}}^{HV})$	$\beta, K, k_1^{eq}, k_2^{eq}$	$K = \frac{k_2^{eq}}{k_{-2}^{eq} a_{H^+}}$ $G = \frac{K k_1^{\mathrm{eq}} a_{\mathrm{H2}}}{k_2^{\mathrm{eq}}}$
TV	$2k_{ad} a_{H_2}(1-\theta_{H_{ad}}^{\mathrm{TV}})^2 - 2k_{des} \theta_{H_{ad}}^{\mathrm{TV}\ 2} - k_2 \theta_{H_{ad}}^{\mathrm{TV}} + k_2 a_{H^+}(1-\theta_{H_{ad}}^{\mathrm{TV}})$	$k_2 \theta_{H_{ad}}^{\mathrm{TV}} - k_{-2} a_{H^+}(1-\theta_{H_{ad}}^{\mathrm{TV}})$	$k_{ad}, k_{des}, \beta, k_2^{eq}$	$B = \sqrt{\frac{a_{\mathrm{H2}} k_{\mathrm{ad}}}{k_{\mathrm{des}}}}$ $Z = \frac{k_2^{\mathrm{eq}}}{k_{\mathrm{des}}}$
HT	$k_1 a_{H_2}(1-\theta_{H_{ad}}^{\mathrm{HT}}) - k_{-1} a_{H^+} \theta_{H_{ad}}^{\mathrm{HT}} + 2k_{ad} a_{H_2}(1-\theta_{H_{ad}}^{\mathrm{HT}})^2 - 2k_{des} \theta_{H_{ad}}^{\mathrm{HT}\ 2}$	$k_1 a_{H_2}(1-\theta_{H_{ad}}^{\mathrm{HT}}) - k_{-1} a_{H^+} \theta_{H_{ad}}^{\mathrm{HT}}$	$k_{ad}, k_{des}, \beta, k_1^{eq}$	B $Y = \frac{a_{\mathrm{H2}} k_1^{\mathrm{eq}}}{k_{\mathrm{des}}}$
HTV	$k_1 a_{H_2}\left(1-\theta_{H_{ad}}^{\mathrm{HTV}}\right) - k_{-1} a_{H^+} \theta_{H_{ad}}^{\mathrm{HTV}} + 2k_{ad} a_{H_2}\left(1-\theta_{H_{ad}}^{\mathrm{HTV}}\right)^2 - 2k_{des} \theta_{H_{ad}}^{\mathrm{HTV}^2} - k_2 \theta_{H_{ad}}^{\mathrm{HTV}} + k_{-2} a_{H^+}\left(1-\theta_{H_{ad}}^{\mathrm{HTV}}\right)$	$k_1 a_{H_2}\left(1-\theta_{H_{ad}}^{\mathrm{HTV}}\right) - k_{-1} a_{H^+} \theta_{H_{ad}}^{\mathrm{HTV}} + k_2 \theta_{H_{ad}}^{\mathrm{HTV}} - k_{-2} a_{H^+}\left(1-\theta_{H_{ad}}^{\mathrm{HTV}}\right)$	$k_{ad}, k_{des}, \beta, k_1^{eq}, k_2^{eq}$	B, Y, Z

Table 3 Parameters derived from each of the mechanisms. Definition of parameters K,G,B,Y and Z given in Table 2.

Mech	$\theta_{H_{ad}}^{eq}$	Limiting reaction order of true j_o[a]		Possible value of α calculated from the "Tafel Slope" $\frac{RT}{F}\frac{\partial log\lvert j\rvert}{\partial \eta}$	Exchange current density, j_o				Limiting H_2 reaction order in the slope of the micropolarisation region[b]
		H^+	H_2		"True": Magnitude of anodic and cathodic currents at $\eta = 0$	Slope of micropolarisation region $\frac{RT}{F}\left(\frac{dj}{d\eta}\right)_{\eta=0}$	Extrapolation from +ve overpotential $j_{\eta\to\infty}(0)$	Extrapolation from -ve overpotential $j_{\eta\to-\infty}(0)$	
HV	$\frac{1}{1+\mathrm{K}}$	-1,0,1	0,1	$(1+\beta), \beta,$ $-(1-\beta), -(2-\beta)$	$F\theta_{H_{ad}}^{HV,eq}\left(Kk_1^{eq}a_{H_2}+k_2^{eq}\right)$	$F\theta_{H_{ad}}^{HV,eq}\left(\frac{1}{\frac{1}{4Kk_1^{\mathrm{eq}}a_{\mathrm{H2}}}+\frac{1}{4k_2^{\mathrm{eq}}}}\right)$	$2F\left(\frac{1}{1+\frac{K}{G}}\right)k_2^{eq}$	$2F\left(\frac{1}{1+GK}\right)Kk_1^{eq}a_{\mathrm{H2}}$[c]	0,1
TV	$\frac{1}{1+\frac{1}{\mathrm{B}}}$	0	0,½	$2, \beta, 0$ $0, -(1-\beta), -2$	$F\theta_{H_{ad}}^{TV,eq}k_2^{eq}$	$F\theta_{H_{ad}}^{TV,eq}\left(\frac{k_2^{\mathrm{eq}}}{\left(1+\frac{Z}{4}+\frac{Z}{4B}\right)}\right)$	$2Fa_{\mathrm{H2}}k_{\mathrm{ad}}$	$2Fk_{des}$	0,½,1
HT	$\frac{1}{1+\frac{1}{\mathrm{B}}}$	0	½,1	$2, \beta, 0$ $0, -(1-\beta)$	$F\theta_{H_{ad}}^{HT,eq}\left(\frac{k_1^{eq}a_{H_2}}{\mathrm{B}}\right)$	$F\theta_{H_{ad}}^{HT,eq}\left(\frac{k_1^{eq}a_{H_2}/B}{\left(1+\frac{Y}{4B}+\frac{Y}{4B^2}\right)}\right)$	$2Fa_{\mathrm{H2}}k_{\mathrm{ad}}$	$2Fk_{des}$	0,½,1
HTV	$\frac{1}{1+\frac{1}{\mathrm{B}}}$	0	0, ½,1	$\sim 2, \beta, 0$ $0, -(1-\beta), \sim -(2-\beta)$	$F\theta_{H_{ad}}^{HTV,eq}\left(\frac{k_1^{\mathrm{eq}}a_{\mathrm{H2}}}{B}+k_2^{\mathrm{eq}}\right)$	$Fk_{\mathrm{des}}\theta_{H_{ad}}^{HTV,eq}\frac{\left(\frac{a_{\mathrm{H2}}k_1^{\mathrm{eq}}}{B}+k_2^{\mathrm{eq}}\left(1+\frac{Y}{B}+\frac{Y}{B^2}\right)\right)}{\left(1+\frac{Z}{4}+\frac{Z+Y}{4B}+\frac{Y}{4B^2}\right)}$	$2F\left(\frac{1}{1+\frac{Z}{Y}}\right)k_2^{\mathrm{eq}}$	$2F\left(\frac{1}{1+\frac{Y}{ZB^2}}\right)\left(\frac{k_1^{\mathrm{eq}}a_{\mathrm{H2}}}{B}\right)$[d]	-½,0,½,1,$^3/_2$

[a] Values represent reaction orders which may occur. Intermediate values may be measured phenomenologically as the mechanism transitions to a different reaction order (i.e. there will be a curved transition range which might be interpreted as an intermediate reaction order).

[b] Reaction order for H^+ the same as for the true exchange current density

[c] via Eq 12, $k_{-1}^{eq}a_{H^+} = Kk_1^{eq}a_{\mathrm{H2}}$, hence the relevance to the *her* is seen.

[d] via Eq 42, $k_{-1}^{\mathrm{eq}}a_{H^+} = \frac{a_{\mathrm{H2}}k_1^{\mathrm{eq}}}{B}$, hence the relevance to the *her* is seen.

Table 4 Fitting parameters and parameters derived from those parameters for the simultaneous fit of all data sets. The derived parameters are calculated under standard conditions, T=298K, a_{H+}=1.0, a_{H2}=1.0. The parameters used for each of the models to fit the data are highlighted in grey. See Appendix B for added notes about the best fit values.

Parameter		**Type**	**Heyrovsky-Volmer**	**Tafel-Volmer**	**Heyrovsky-Tafel-Volmer**
#Fit parameters			5	5	6
Fit domain			-50mV – 50 mV	-50mV – 100 mV	-50mV – 100 mV
β		Fixed	0.33	0.52	0.71
$K^{\ominus}$		Fit	3.09	N.A	N.A
$G^{\ominus}$		Fit	0.52	N.A	N.A
$B^{\ominus}$		Fit	N.A	0.28	0.31
$Y^{\ominus}$		Fit	N.A	N.A.	0.0072
$Z^{\ominus}$		Fit	N.A	0.42	1.27
$k_{des}^{\ominus}$/ mol cm^{-2} s^{-1}		Fit	N.A	2.1×10^{-5}	1.1×10^{-5}
E_a / kJ mol^{-1}		Fit	1.8×10^{4}	2.3×10^{4}	2.0×10^{4}
$\theta_{H_{ad}}^{eq,\ominus}$		Derived	0.24	0.22	0.237
$\theta_{H_{ad}}^{\ominus}(\eta \to -\infty)$		Derived	0.38	1	0.944
$\theta_{H_{ad}}^{\ominus}(\eta \to \infty)$		Derived	0.14	0	0.006
$\Delta_{ads}G_{H_2,opd}^{\ominus}$/ kJ mol^{-1}		Derived	4.4	3.1	2.9
$k_1^{\ominus}$/ mol cm^{-2} s^{-1}		Derived	8.6×10^{-7}	N.A	8.0×10^{-8}
$k_2^{\ominus}$/ mol cm^{-2} s^{-1}		Derived/Fit[b]	5.1×10^{-6}	8.9×10^{-6}	1.4×10^{-5}
$k_{ad}^{\ominus}$/ mol cm^{-2} s^{-1}		Derived	N.A	1.7×10^{-6}	1.1×10^{-6}
$k_1^{\ominus}$/ cm s^{-1}		Derived[a]	1.7	N.A	0.16
$k_{ad}^{\ominus}$/ cm s^{-1}		Derived[a]	N.A	3.4	2.1
$k_{des}^{\ominus}$/ cm s^{-1}		Derived	N.A	41.3	21.6
$j_0^{\ominus}$ /mA cm^{-2}	"True"		183	189	325	325
	Micropolarisation		165	129	151	151
	Extrapolated from j(∞)		142	329	15	15
	Extrapolated from j(-∞)		197	4060	47	47

[a] Calculated using the saturated concentration of hydrogen in electrolyte 5.1×10^{-7} mol cm^{-3} [b]Fit parameter for Heyrovsky-Volmer

Figure 1 Representative plots showing the characteristic shapes of the four different models studied in this paper (a) Heyrovsky-Volmer; (b) Tafel-Volmer; (c) Heyrovsky-Tafel; (d) Heyrovsky-Tafel-Volmer. Values for producing the plots are displayed directly on them and are chosen to illustrate various features of the mechanisms. The main plots show both the current density (left axis) and hydrogen coverage(right axis). Inset in the graphs are the $log|j| vs\ \eta$ plots for the corresponding currents and Tafel slopes (dotted lines, multiplied by $\frac{RT}{F}$) in terms of the β used to generate the data. Also shown on the inset plots are the component currents associated with electrochemical Eq 3-Eq 6 as appropriate. These plots do not represent a specific system, but are more included to highlight the different facets of the alternative mechanisms.

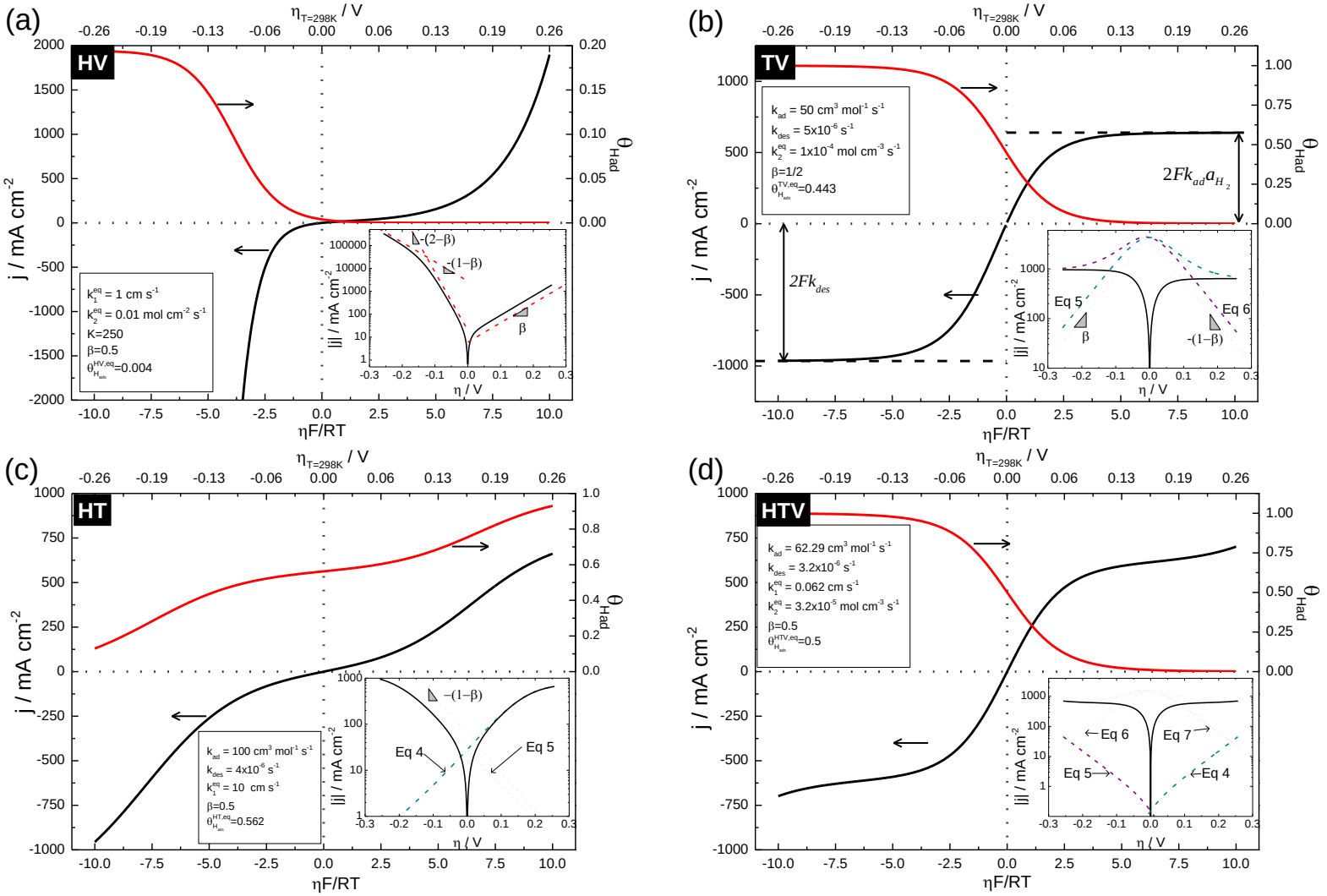

Figure 2 Variation of the mathematically determined hydrogen adsorption isotherm, $\theta_{H_{ad}}^{\mathrm{HV}}$, (Eq 15) and scaled current, $\frac{j^{HV}}{k_2^{eq}}$, (Eq 19) for the Heyrovsky-Volmer reaction as a function of dimensionless overpotential and the parameters *K*, and *G*. (a) $\theta_{H_{ad}}^{\mathrm{HV}}$ as a function of G at constant K/a_{H^+}; (b) $\theta_{H_{ad}}^{\mathrm{HV}}$ as a function of K at constant G, and (c) $\theta_{H_{ad}}^{\mathrm{HV}}$ at a constant ratio of G to K. (d)-(f)scaled $\frac{j^{HV}}{k_2^{eq}}$ plots for the same values of $\theta_{H_{ad}}^{\mathrm{HV}}$ and parameters in (a)-(c). The calculated slopes of the dotted lines in d,e and f correspond to $\frac{\mathrm{RT}}{F}\frac{d\mathrm{Log}_e|j|}{\mathrm{d}\eta}$ and are displayed in terms of β, the mechanistic symmetry factor. Plots are produced with β=1/2. $K = \frac{k_2^{eq}}{k_{-2}^{eq}c_{H^+}}$ and $G = \frac{Kk_1^{\mathrm{eq}}c_{\mathrm{H2}}}{k_2^{\mathrm{eq}}}$. The top x-axis provides the overpotential values when T=298K.

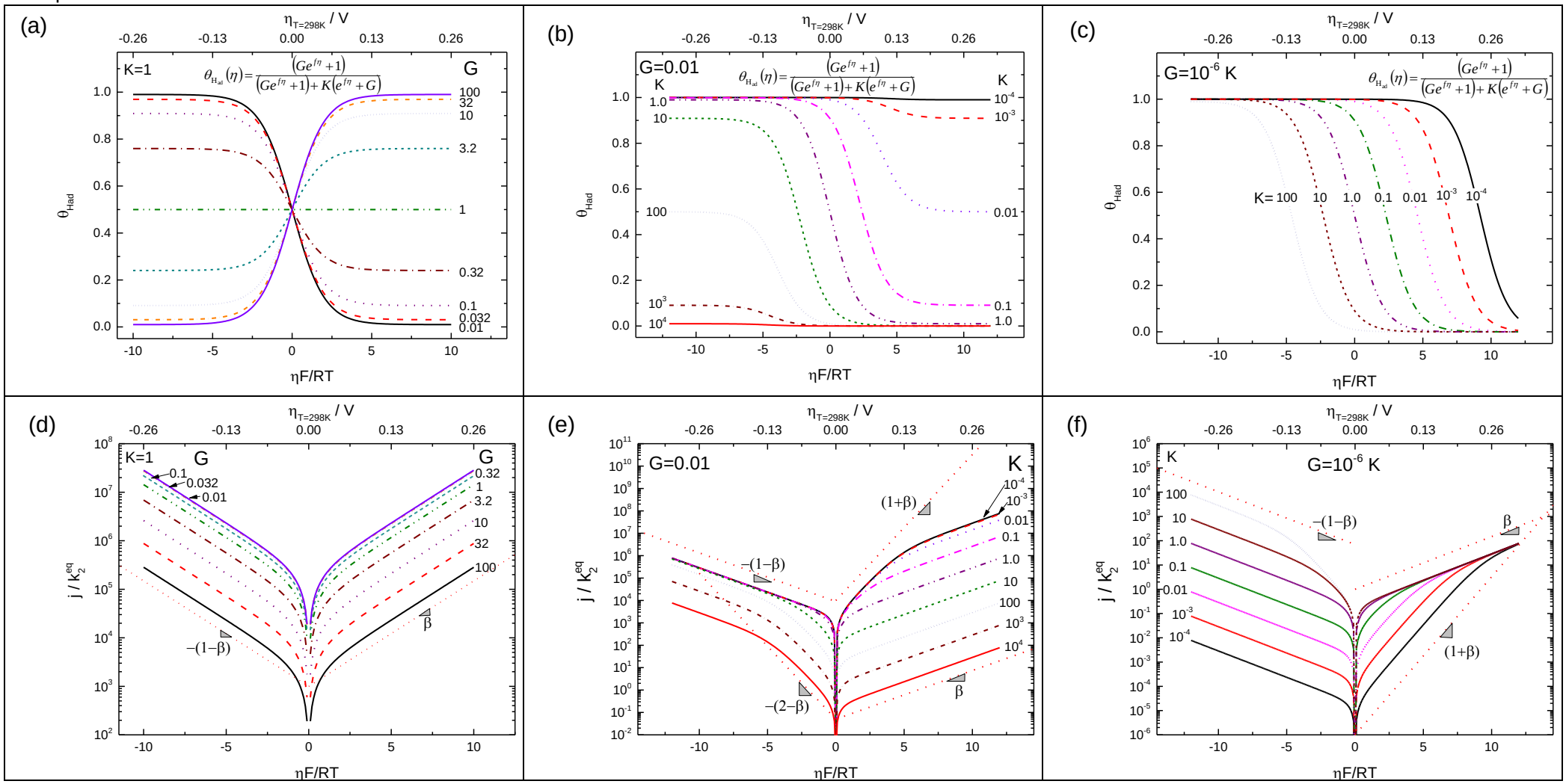

Figure 3 Variation of the mathematically determined hydrogen adsorption isotherm, $\theta_{H_{ad}}^{\mathrm{TV}}$, (Eq 27) and scaled current, $\frac{j^{TV}}{k_{des}}$, (Eq 30) for the Tafel-Volmer reaction as a function of dimensionless overpotential and parameters *B* and *Z*. (a) $\theta_{H_{ad}}^{\mathrm{TV}}$ for *Z*=1, and different values of *B*; (b) $\theta_{H_{ad}}^{\mathrm{TV}}$ for B=1, and different values of *Z*; (c) $\theta_{H_{ad}}^{\mathrm{TV}}$ at a constant ratio of *B* to *Z*. (d)-(f) $\frac{j^{TV}}{k_{des}}$ plots for the same values of $\theta_{H_{ad}}^{\mathrm{TV}}$ and parameters in (a)-(c).The calculated slopes of the dotted lines correspond to $\frac{\mathrm{RT}}{F}\frac{d\mathrm{Log}_e|j|}{\mathrm{d}\eta}$ and are displayed in terms of β, the mechanistic symmetry factor. $B = \sqrt{\frac{c_{\mathrm{H_2}}k_{\mathrm{ad}}}{k_{\mathrm{des}}}}$ and $Z = \frac{k_2^{\mathrm{eq}}}{k_{\mathrm{des}}}$. Plots are produced with β=1/2. The top x-axis provides the overpotential values when T=298K.

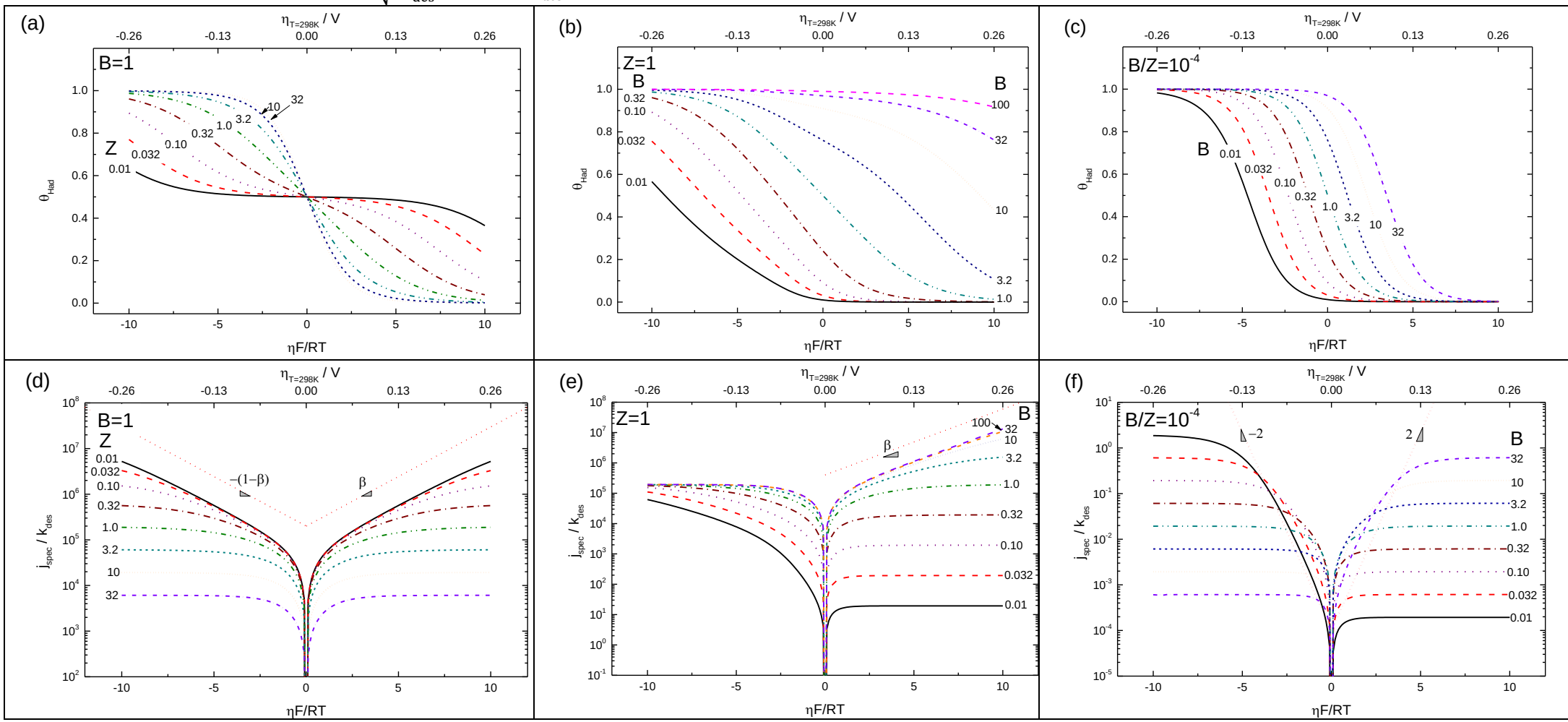

Figure 4 Variation of the mathematically determined hydrogen adsorption isotherm, $\theta_{H_{ad}}^{\mathrm{HT}}$, (Eq 36) and scaled current, $\frac{j^{HT}}{k_{des}}$, (Eq 39) for the Heyrovsky-Tafel reaction as a function of dimensionless overpotential and parameters *B* and *Y*. (a) $\theta_{H_{ad}}^{\mathrm{HT}}$ for *B*=1, and different values of *Y*; (b) $\theta_{H_{ad}}^{\mathrm{TV}}$ for Y=1, and different values of *B*; (c) $\theta_{H_{ad}}^{\mathrm{HT}}$ at a constant ratio of *B* to *Y*. (d)-(f) $\frac{j^{HT}}{k_{des}}$ plots for the same values of $\theta_{H_{ad}}^{\mathrm{HT}}$ and parameters in (a)-(c).The calculated slopes of the dotted lines correspond to $\frac{\mathrm{RT}}{F}\frac{d\mathrm{Log}_e|j|}{\mathrm{d}\eta}$ and are displayed in terms of β, the mechanistic symmetry factor. $B=\sqrt{\frac{c_{\mathrm{H2}}k_{\mathrm{ad}}}{k_{\mathrm{des}}}}$, $Y=\frac{c_{\mathrm{H2}}k_1^{\mathrm{eq}}}{k_{\mathrm{des}}}$. Plots are produced with β=1/2. The top x-axis provides the overpotential values when T=298K.

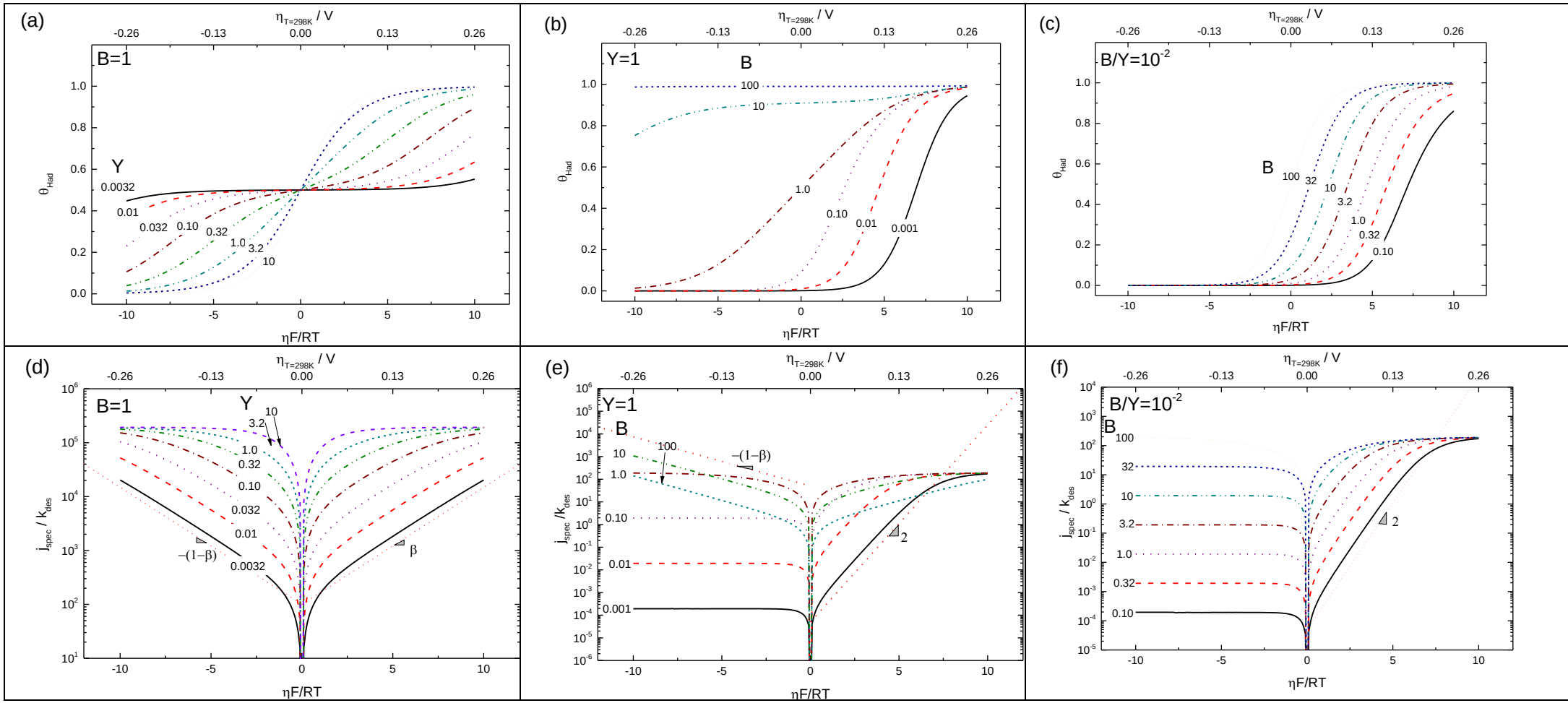

Figure 5 Variation of the mathematically determined hydrogen adsorption isotherm, $\theta_{H_{ad}}^{\mathrm{HTV}}$, (Eq 43) and scaled current, $\frac{j^{HTV}}{k_{des}}$, (Eq 47) for the Heyrovsky-Tafel-Volmer reaction as a function of dimensionless overpotential and parameters *B, Y*, and *Z.* (a) $\theta_{H_{ad}}^{\mathrm{HTV}}$ for *Y=10^{-4}, Z=1* , and different values of *B*; (b) $\theta_{H_{ad}}^{\mathrm{HTV}}$ for *B=1, Z=0.1* and different values of *Y*; (c) $\theta_{H_{ad}}^{\mathrm{HTV}}$ for *Z=10* and a constant ratio of *B* to *Y* (B/Y=10). (d)-(f) $\frac{j^{HTV}}{k_{des}}$ plots for the same values of $\theta_{H_{ad}}^{\mathrm{HTV}}$ and parameters in (a)-(c).The calculated slopes of the dotted lines correspond to $\frac{\mathrm{RT}}{F}\frac{d\mathrm{Log}_e|j|}{\mathrm{d}\eta}$ and are displayed in terms of β, the mechanistic symmetry factor. $B = \sqrt{\frac{c_{\mathrm{H2}}k_{\mathrm{ad}}}{k_{\mathrm{des}}}}$, $Y = \frac{c_{\mathrm{H2}}k_1^{\mathrm{eq}}}{k_{\mathrm{des}}}$, and $Z = \frac{k_2^{\mathrm{eq}}}{k_{\mathrm{des}}}$. Plots are produced with β=1/2. The top x-axis provides the overpotential values when T=298K.

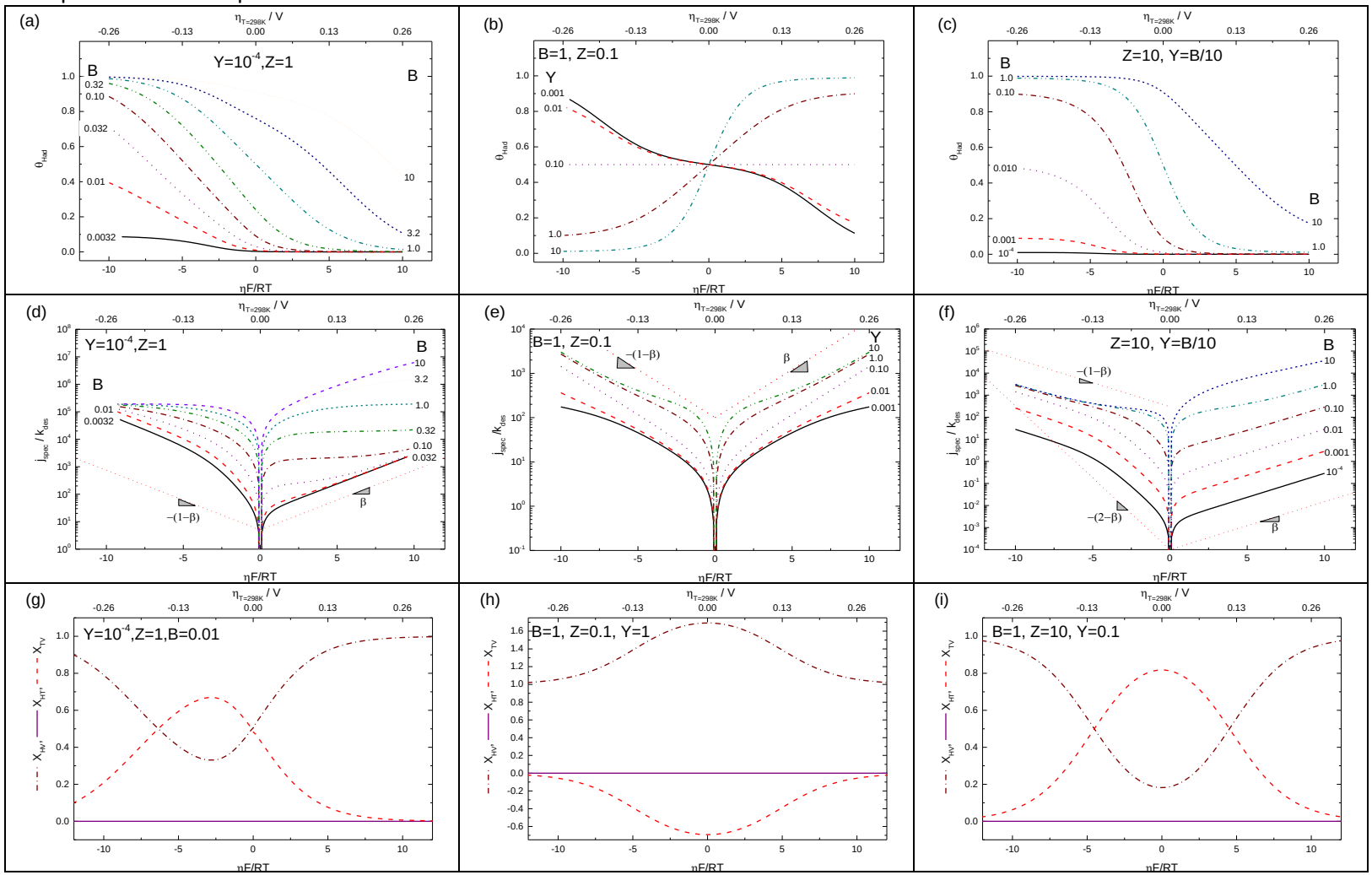

Figure 6 Experimental results for the *her/hor* utilising a number of different experimental techniques. Microelectrodes with high surface area platinum catalyst (R_f=30) in contact with Nafion or acid (details in [45]); a 50 μm platinum microelectrode (R_f ≈1) in contact with aqueous acid (details in [19]), a single platinum particle (450 nm in diameter) in acid (details in [19]) , to a Pt rotating disk electrode disk (R_f ≈1, 7000 rpm) in contact with 0.1 mol dm^{-3} $HClO_4$, and results obtained utilising our floating electrode technique[16, 32] (R_f≈1) for an electrode in 1 mol dm^{-3} $HClO_4$. T=298K, dV/dt=10 mV s^{-1}, solution saturated with 1 bar hydrogen.

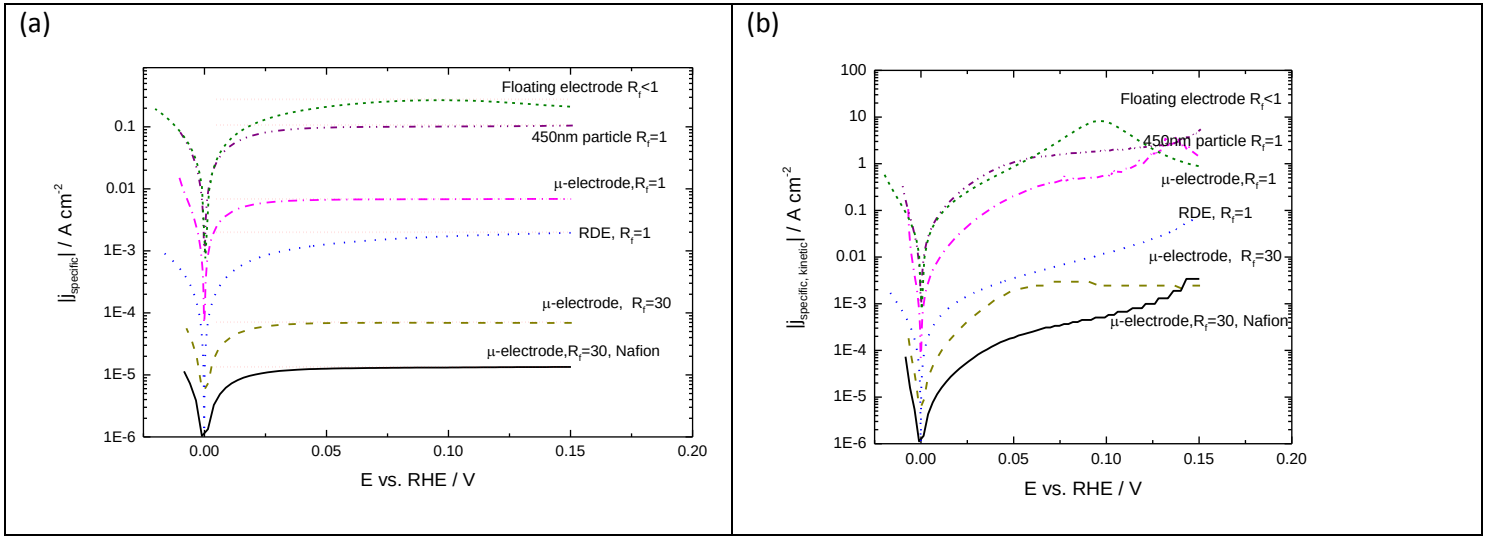

Figure 7 Experimental results for the *her/hor* utilising the floating electrode technique[16, 32]. (a) Temperature dependence of a 2.2 μg_{Pt} cm^{-2} HiSpec 9100 60 % Pt/C electrode in 4 mol dm^{-3} $HClO_4$ 1 bar H_2(uncorrected for water vapour), Temperature: 278K, 288K, 298K, 303K,313K, 323K, 333K, 10 mV s^{-1}, positive going scan. (b) Hydrogen partial pressure dependence of a 3.5 μg_{Pt} cm^{-2} HiSpec 9100 60 % Pt/C electrode in 0.5 mol dm^{-3} $HClO_4$. H_2 partial pressure (N_2 diluent, uncorrected for water vapour): 0.126, 0.106, 0.087, 0.068, 0.048, 0.029; 298K, 10 mV s^{-1}, positive going scan. (c) Data in (a) and (b) plotted together on a logarithmic current scale. The potential scale on the x-axis has been converted to RHE, accounting for the change in equilibrium potential with hydrogen partial pressure through the Nernst equation. Currents are corrected to the nominal Pt surface area calculated using the hydrogen adsorption charge. Both (a) and (b) also show RDE results for a platinum disk in 0.1 mol dm^{-3} $HClO_4$ saturated in hydrogen gas at a rotation rate of 7000 rpm.

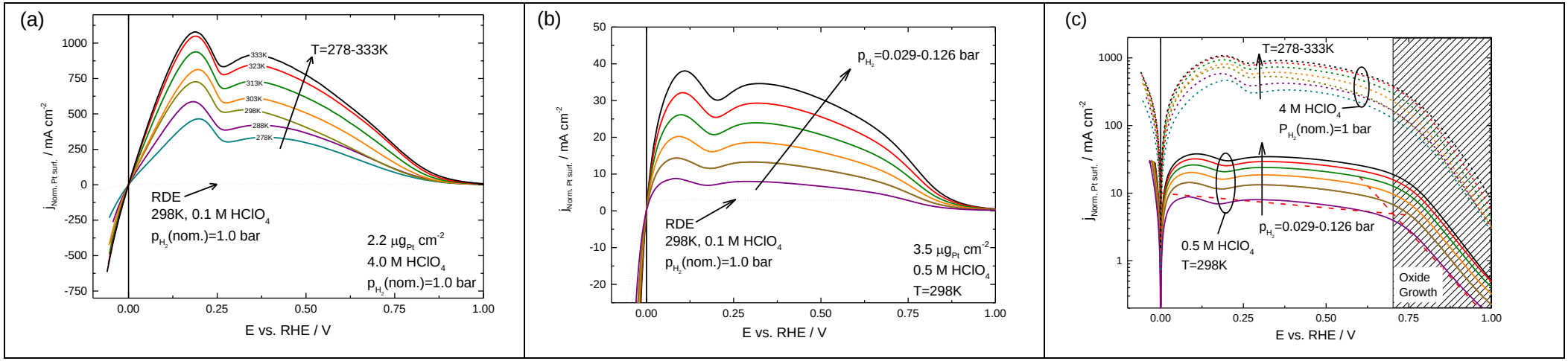

Figure 8 Simultaneous fits (using a common set of parameters) for the data set given in Figure 7(a)&(b) using the (a) Heyrovsky-Volmer mechanism (Eq 19, fit performed between -0.05..0.05 V); Tafel-Volmer mechanism (Eq 30, fit performed between -0.05..0.10 V) and (c) Heyrovsky-Tafel-Volmer mechanism (Eq 47, fit performed between -0.05..0.10 V). For all fits, β was set to ½ and the hydrogen partial pressures were corrected for saturated water vapour pressure at the appropriate temperature of the reaction. All data were fit simultaneously with the fit parameters displayed on the diagrams along with the equilibrium hydrogen coverage derived from the fit parameters. Details of data sets given in caption to Figure 7. Symbols: Data, Dashed line: Fit.

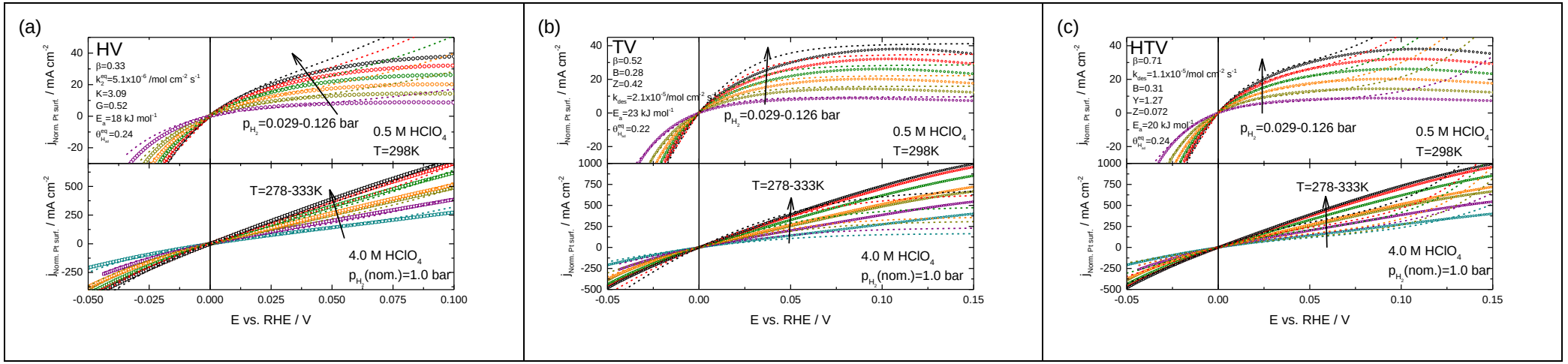

Figure 9 Calculated *hor/her* curves for the fits calculated using the different mechanisms in this paper and the fitting parameters derived in Figure 8. (a) Heyrovsky-Volmer mechanism (Eq 19, fit performed between -0.05..0.05 V); (b) Tafel-Volmer mechanism (Eq 30, fit performed between -0.05..0.10 V) and (c); Heyrovsky-Tafel-Volmer mechanism (Eq 47, fit performed between -0.05..0.10 V). (d) shows the breakdown of pathways for the *hor/her* as a function of overpotential for the Heyrovsky-Tafel-Volmer mechanism displayed in (c) based upon Eq 51, Eq 52 and Eq 53. For all fits the hydrogen partial pressures were corrected for saturated water vapour pressure at the appropriate temperature of the reaction. Parameters for the fits are the same as shown in Figure 8 and Table 4. a_{H^+}=1, a_{H_2}=1, T=298K. For the HV and HTV reactions we also plot the asymptotic hydrogen coverage at large positive and negative overpotentials. We also plot the observed Tafel slope as a function of potential, including the expected Tafel slope based on the β-value determined from the fit and temperature (298K), (e.g. 118 mV decade^{-1} when β=½). The part-currents associated with each stpe of the mechanisms are – Forward Heyrovsky (-----), Reverse Heyrovsky (·····). Forward Volmer (-·-·-·), Reverse Volmer (·····).

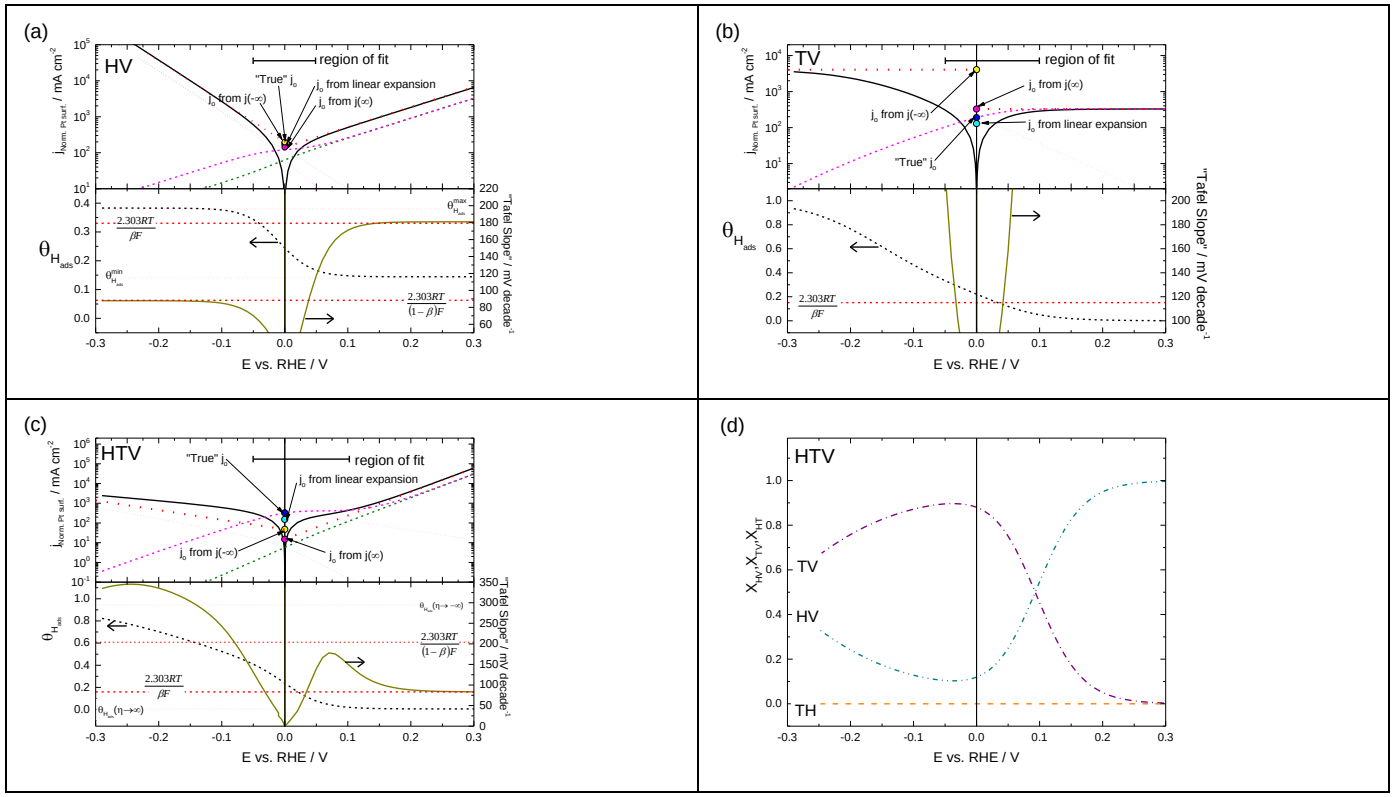

References

1. Xiao, P.; Sk, M. A.; Thia, L.; Ge, X.; Lim, R. J.; Wang, J.-Y.; Lim, K. H.; Wang, X., Molybdenum Phosphide as an Efficient Electrocatalyst for the Hydrogen Evolution Reaction *Energy Environ. Sci.* **2014**, *7*, 2624-2629.
2. Popczun, E. J.; Read, C. G.; Roske, C. W.; Lewis, N. S.; Schaak, R. E., Highly Active Electrocatalysis of the Hydrogen Evolution Reaction by Cobalt Phosphide Nanoparticles. *Angew. Chem.-Int. Edit.* **2014**, *53*, 5427-5430.
3. Benck, J. D.; Chen, Z. B.; Kuritzky, L. Y.; Forman, A. J.; Jaramillo, T. F., Amorphous Molybdenum Sulfide Catalysts for Electrochemical Hydrogen Production: Insights into the Origin of Their Catalytic Activity. *ACS Catalysis* **2012**, *2*, 1916-1923.
4. Kucernak, A. R. J.; Naranammalpuram Sundaram, V. N., Nickel Phosphide: The Effect of Phosphorus Content on Hydrogen Evolution Activity and Corrosion Resistance in Acidic Medium. *Journal of Materials Chemistry A* **2014**, *2*, 17435-17445.
5. Gasteiger, H. A.; Panels, J. E.; Yan, S. G., Dependence of Pem Fuel Cell Performance on Catalyst Loading. *Journal of Power Sources* **2004**, *127*, 162-171.
6. Bagotzky, V. S.; Osetrova, N. V., Investigations of Hydrogen Ionization on Platinum with the Help of Micro-Electrodes. *Journal of Electroanalytical Chemistry and Interfacial Electrochemistry* **1973**, *43*, 233-249.
7. Chen, S.; Kucernak, A., Electrocatalysis under Conditions of High Mass Transport: Investigation of Hydrogen Oxidation on Single Submicron Pt Particles Supported on Carbon. *The Journal of Physical Chemistry B* **2004**, *108*, 13984-13994.
8. Sun, Y.; Lu, J.; Zhuang, L., Rational Determination of Exchange Current Density for Hydrogen Electrode Reactions at Carbon-Supported Pt Catalysts. *Electrochimica Acta* **2010**, *55*, 844-850.
9. Durst, J.; Siebel, A.; Simon, C.; Hasche, F.; Herranz, J.; Gasteiger, H. A., New Insights into the Electrochemical Hydrogen Oxidation and Evolution Reaction Mechanism. *Energy & Environmental Science* **2014**, *7*, 2255-2260.
10. Varcoe, J. R., et al., Anion-Exchange Membranes in Electrochemical Energy Systems. *Energy & Environmental Science* **2014**, *7*, 3135-3191.
11. Rossmeisl, J.; Chan, K.; Skúlason, E.; Björketun, M. E.; Tripkovic, V., On the Ph Dependence of Electrochemical Proton Transfer Barriers. *Catalysis Today* **2016**, *262*, 36-40.
12. Tafel, J., *Z. Phys. Chem. Stoechiom. Verwandtschafts.* **1905** *50*, 641
13. Heyrovsky, J., *Recl. Trav. Chim. Pays-Bas* **1927** *46* 582
14. Volmer, T.; Erdey-Gruz, M., *Z. Phys. Chem., Abt. A* **1930** *150*, 203
15. Vogel, W.; Lundquist, J.; Ross, P.; Stonehart, P., Reaction Pathways and Poisons .2. Rate Controlling Step for Electrochemical Oxidation of Hydrogen on Pt in Acid and Poisoning of Reaction by Co. *Electrochimica Acta* **1975**, *20*, 79-93.
16. Zalitis, C. M.; Kramer, D.; Sharman, J.; Wright, E.; Kucernak, A. R., Pt Nano-Particle Performance for Pefc Reactions at Low Catalyst Loading and High Reactant Mass Transport. *ECS Transactions* **2013**, *58*, 39-47.
17. Zalitis, C. M.; Kramer, D.; Kucernak, A. R., Electrocatalytic Performance of Fuel Cell Reactions at Low Catalyst Loading and High Mass Transport. *Physical Chemistry Chemical Physics* **2013**, *15*, 4329-4340.
18. Wesselmark, M.; Wickman, B.; Lagergren, C.; Lindbergh, G., Hydrogen Oxidation Reaction on Thin Platinum Electrodes in the Polymer Electrolyte Fuel Cell. *Electrochemistry Communications* **2010**, *12*, 1585-1588.
19. Chen, S. L.; Kucernak, A., Electrocatalysis under Conditions of High Mass Transport: Investigation of Hydrogen Oxidation on Single Submicron Pt Particles Supported on Carbon. *Journal of Physical Chemistry B* **2004**, *108*, 13984-13994.
20. Dechialvo, M. R. G.; Chialvo, A. C., Hydrogen Evolution Reaction - Analysis of the Volmer-Heyrovsky-Tafel Mechanism with a Generalized Adsorption Model. *Journal of Electroanalytical Chemistry* **1994**, *372*, 209-223.
21. de Chialvo, M. R. G.; Chialvo, A. C., Existence of Two Sets of Kinetic Parameters in the Correlation of the Hydrogen Electrode Reaction. *Journal of the Electrochemical Society* **2000**, *147*, 1619-1622.
22. Quaino, P. M.; de Chialvo, M. R. G.; Chialvo, A. C., Hydrogen Diffusion Effects on the Kinetics of the Hydrogen Electrode Reaction - Part Ii. Evaluation of Kinetic Parameters. *Physical Chemistry Chemical Physics* **2004**, *6*, 4450-4455.
23. Marozzi, C. A.; Canto, M. R.; Costanza, V.; Chialvo, A. C., Analysis of the Use of Voltammetric Results as a Steady State Approximation to Evaluate Kinetic Parameters of the Hydrogen Evolution Reaction. *Electrochimica Acta* **2005**, *51*, 731-738.
24. Quaino, P. M.; Gennero de Chialvo, M. R.; Chialvo, A. C., Kinetic Study of the Hydrogen Electrode Reaction on Bi-Modified Platinum. *Journal of the Electrochemical Society* **2009**, *156*, B167-B173.

25. Montero, M. A.; de Chialvo, M. R. G.; Chialvo, A. C., Hydrogen Oxidation Reaction on Platinum Nanoparticles: Transition between Mechanistic Routes. *Electrochemistry Communications* **2010**, *12*, 398-401.
26. Arce, M. D.; Bonazza, H. L.; Fernandez, J. L., Kinetic Analysis of the Hydrogen Electrode Reaction in Unbuffered Media. Theory and Studies on Pt Microelectrodes. *Electrochimica Acta* **2013**, *107*, 248-260.
27. Wang, J. X.; Springer, T. E.; Adzic, R. R., Dual-Pathway Kinetic Equation for the Hydrogen Oxidation Reaction on Pt Electrodes. *Journal of The Electrochemical Society* **2006**, *153*, A1732-A1740.
28. Gennero de Chialvo, M. R.; Chialvo, A. C., Hydrogen Diffusion Effects on the Kinetics of the Hydrogen Electrode Reaction. Part I. Theoretical Aspects. *Physical Chemistry Chemical Physics* **2004**, *6*, 4009-4017.
29. Rau, M. S.; Gennero de Chialvo, M. R.; Chialvo, A. C., Kinetic Study of the Hydrogen Oxidation Reaction on Pt over the Complete Overpotential Range. *Journal of Power Sources* **2013**, *229*, 210-215.
30. Quaino, P. M.; de Chialvo, M. R. G.; Chialvo, A. C., Hydrogen Electrode Reaction: A Complete Kinetic Description. *Electrochimica Acta* **2007**, *52*, 7396-7403.
31. Certificate of Analysis. Correspondence with Johnson Matthey Fuel Cells: 16 Dec 2009.
32. Zalitis, C. M.; Sharman, J.; Wright, E.; Kucernak, A. R., Properties of the Hydrogen Oxidation Reaction on Pt/C Catalysts at Optimised High Mass Transport Conditions and Its Relevance to the Anode Reaction in Pefcs and Cathode Reactions in Electrolysers. *Electrochimica Acta* **2015**, *176*, 763-776.
33. Kucernak, A. R.; Toyoda, E., Studying the Oxygen Reduction and Hydrogen Oxidation Reactions under Realistic Fuel Cell Conditions. *Electrochemistry Communications* **2008**, *10*, 1728-1731.
34. Kucernak, A., Doi to Be Provided at Proofing Stage. 2016.
35. Guidelli, R.; Compton, R. G.; Feliu, J. M.; Gileadi, E.; Lipkowski, J.; Schmickler, W.; Trasatti, S., Defining the Transfer Coefficient in Electrochemistry: An Assessment (Iupac Technical Report). *Pure and Applied Chemistry* **2014**, *86*, 245-258.
36. Breiter, M. W., In *Handbook of Fuel Cells: Fundamentals, Technology and Application*, John Wiley & Sons: New York 2003; Vol. 2, p 361.
37. Gennero de Chialvo, M. R.; Chialvo, A. C., The Tafel–Heyrovsky Route in the Kinetic Mechanism of the Hydrogen Evolution Reaction. *Electrochemistry Communications* **1999**, *1*, 379-382.
38. Quaino, P. M.; Fernandez, J. L.; de Chialvo, M. R. G.; Chialvo, A. C., Hydrogen Oxidation Reaction on Microelectrodes: Analysis of the Contribution of the Kinetic Routes. *Journal of Molecular Catalysis a-Chemical* **2006**, *252*, 156-162.
39. Markovic, N. M.; Sarraf, S. T.; Gasteiger, H. A.; Ross, P. N., Hydrogen Electrochemistry on Platinum Low-Index Single-Crystal Surfaces in Alkaline Solution. *Journal of the Chemical Society-Faraday Transactions* **1996**, *92*, 3719-3725.
40. Sheng, W. C.; Gasteiger, H. A.; Shao-Horn, Y., Hydrogen Oxidation and Evolution Reaction Kinetics on Platinum: Acid Vs Alkaline Electrolytes. *Journal of the Electrochemical Society* **2010**, *157*, B1529-B1536.
41. Rheinlander, P. J.; Herranz, J.; Durst, J.; Gasteiger, H. A., Kinetics of the Hydrogen Oxidation/Evolution Reaction on Polycrystalline Platinum in Alkaline Electrolyte Reaction Order with Respect to Hydrogen Pressure. *Journal of the Electrochemical Society* **2014**, *161*, F1448-F1457.
42. Conway, B. E.; Jerkiewicz, G., Nature of Electrosorbed H and Its Relation to Metal Dependence of Catalysis in Cathodic H-2 Evolution. *Solid State Ionics* **2002**, *150*, 93-103.
43. Parsons, R., The Rate of Electrolytic Hydrogen Evolution and the Heat of Adsorption of Hydrogen. *Transactions of the Faraday Society* **1958**, *54*, 1053-1063.
44. Neyerlin, K. C.; Gu, W.; Jorne, J.; Gasteiger, H. A., Study of the Exchange Current Density for the Hydrogen Oxidation and Evolution Reactions. *Journal of The Electrochemical Society* **2007**, *154*, B631-B635.
45. Jiang, J. H.; Kucernak, A., Investigations of Fuel Cell Reactions at the Composite Microelectrode Vertical Bar Solid Polymer Electrolyte Interface. I. Hydrogen Oxidation at the Nanostructured Pt Vertical Bar Nafion((R)) Membrane Interface. *Journal of Electroanalytical Chemistry* **2004**, *567*, 123-137.
46. Iden, H.; Kucernak, A. R., Analysis of Effective Surface Area for Electrochemical Reaction Derived from Mass Transport Property. *Journal of Electroanalytical Chemistry* **2014**, *734*, 61-69.
47. Montero, M. A.; de Chialvo, M. R. G.; Chialvo, A. C., Rotating Nanoparticle Array Electrode for the Kinetic Study of Reactions under Mixed Control. *Electrochimica Acta* **2010**, *56*, 756-761.
48. Bonazza, H. L.; Vega, L. D.; Fernandez, J. L., Analysis of the Hydrogen Electrode Reaction Mechanism in Thin-Layer Cells. 2. Study of Hydrogen Evolution on Microelectrodes by Scanning Electrochemical Microscopy. *Journal of Electroanalytical Chemistry* **2014**, *713*, 9-16.

49. Zhou, J. F.; Zu, Y. B.; Bard, A. J., Scanning Electrochemical Microscopy Part 39. The Proton/Hydrogen Mediator System and Its Application to the Study of the Electrocatalysis of Hydrogen Oxidation. *Journal of Electroanalytical Chemistry* **2000**, *491*, 22-29.
50. Zoski, C. G., Scanning Electrochemical Microscopy: Investigation of Hydrogen Oxidation at Polycrystalline Noble Metal Electrodes. *The Journal of Physical Chemistry B* **2003**, *107*, 6401-6405.
51. Neyerlin, K. C.; Gu, W. B.; Jorne, J.; Gasteiger, H. A., Study of the Exchange Current Density for the Hydrogen Oxidation and Evolution Reactions. *Journal of the Electrochemical Society* **2007**, *154*, B631-B635.
52. Markiewicz, M.; Zalitis, C.; Kucernak, A., Performance Measurements and Modelling of the Orr on Fuel Cell Electrocatalysts - the Modified Double Trap Model. *Electrochimica Acta* **2015**, *179*, 126-136.
53. Trasatti, S., Work Function, Electronegativity, and Electrochemical Behaviour of Metals: Iii. Electrolytic Hydrogen Evolution in Acid Solutions. *Journal of Electroanalytical Chemistry and Interfacial Electrochemistry* **1972**, *39*, 163-184.
54. Montero, M. A.; Fernandez, J. L.; de Chialvo, M. R. G.; Chialvo, A. C., Kinetic Study of the Hydrogen Oxidation Reaction on Nanostructured Iridium Electrodes in Acid Solutions. *Journal of Physical Chemistry C* **2013**, *117*, 25269-25275.

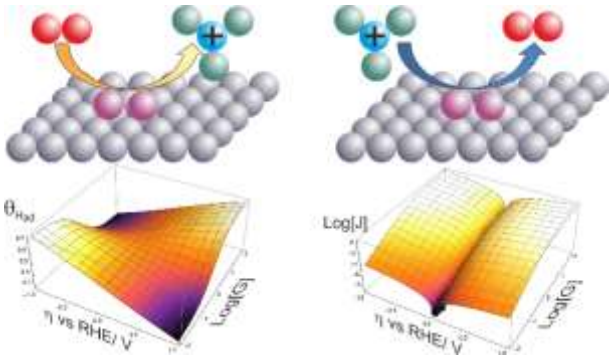
θHad
η vs RHE/ V
Log[G]
Log[J]
η vs RHE/ V
Log[G]